HHS Public Access

Author manuscript

AJR Am J Roentgenol. Author manuscript; available in PMC 2024 January 30.

Published in final edited form as:

AJR Am J Roentgenol. 2023 December ; 221(6): 788–804. doi:10.2214/AJR.23.29342.

Use of a Commercial 7-T MRI Scanner for Clinical Brain Imaging: Indications, Protocols, Challenges, and Solutions—A Single-Center Experience

Can Özütemiz, MD[1], **Matthew White, BA, RT**[2,3], **Wendy Elvendahl, BS, RT**[2,3], **Yigitcan Eryaman, PhD**[2], **Małgorzata Marjańska, PhD**[2], **Gregory J. Metzger, PhD**[2], **Rémi Patriat, PhD**[2], **Jeramy Kulesa, MS**[2], **Noam Harel, PhD**[2], **Yoichi Watanabe, PhD**[4], **Andrea Grant, PhD**[2], **Guglielmo Genovese, PhD**[2], **Zuzan Cayci, MD**[1,3]

[1]Department of Radiology, University of Minnesota, 420 Delaware St SE, MMC 292, Minneapolis, MN 55455.

[2]Center for Magnetic Resonance Research, Department of Radiology, University of Minnesota, Minneapolis, MN.

[3]Center for Clinical Imaging Research, Department of Radiology, University of Minnesota, Minneapolis, MN.

[4]Department of Radiation Oncology, University of Minnesota, Minneapolis, MN.

Abstract

The first commercially available 7-T MRI scanner (Magnetom Terra) was approved by the FDA in 2017 for clinical imaging of the brain and knee. After initial protocol development and sequence optimization efforts in volunteers, the 7-T system, in combination with an FDA-approved 1-channel transmit/32-channel receive array head coil, can now be routinely used for clinical brain MRI examinations. The ultrahigh field strength of 7-T MRI has the advantages of improved spatial resolution, increased SNR, and increased CNR but also introduces an array of new technical challenges. The purpose of this article is to describe an institutional experience with the use of the commercially available 7-T MRI scanner for routine clinical brain imaging. Specific clinical indications for which 7-T MRI may be useful for brain imaging include brain tumor evaluation with possible perfusion imaging and/or spectroscopy, radiotherapy planning; evaluation of multiple sclerosis and other demyelinating diseases, evaluation of Parkinson disease and guidance of deep brain stimulator placement, high-detail intracranial MRA and vessel wall imaging, evaluation of pituitary pathology, and evaluation of epilepsy. Detailed protocols,

Address correspondence to C. Özütemiz (ozutemiz@umn.edu, @CanOzutemiz).

Provenance and review: Not solicited; externally peer reviewed.

Peer reviewers: Ibrahim Tuna, University of Florida; Christie M. Lincoln, Baylor College of Medicine; Gaurang Shah, University of Michigan; Jason M. Johnson, The University of Texas MD Anderson Cancer Center; additional individual(s) who chose not to disclose their identity.

Based on a presentation at the Radiological Society of North America 2022 annual meeting, Chicago, IL.

R. Patriat is a consultant for Surgical Information Sciences, Inc. N. Harel is a cofounder of Surgical Information Sciences, Inc. The remaining authors declare that there are no other disclosures relevant to the subject matter of this article.

including sequence parameters, for these various indications are presented, and implementation challenges (including artifacts, safety, and side effects) and potential solutions are explored.

Keywords

7 T; brain imaging; MRI; neuroradiology

The first commercially available 7-T MRI scanner (Magnetom Terra, Siemens Healthineers) was approved by the FDA in 2017 for clinical imaging of the brain and knee [1]. This 7-T MRI system was installed at our institution in 2020. Because of the limited nature of the vendor-supplied neuroimaging sequences and the lack of published standardized 7-T routine brain MRI protocols (including detailed acquisition parameters), we conducted protocol development and sequence optimization in healthy volunteers and selected patients over a 12-month period, beginning in May 2021. As the result of these efforts, we now routinely use the 7-T system for clinical brain MRI examinations. All such examinations are performed with a 1-channel transmit/32-channel receive array head coil (Nova Medical), which currently is the only FDA-approved commercially available head coil for use with this 7-T system. The ultrahigh field strength of 7 T has the advantages of improved spatial resolution, increased SNR, and increased CNR [2] but also introduces technical challenges. We describe our institutional experience in the use of a commercially available 7-T MRI scanner for routine clinical brain imaging. We discuss clinical indications for which 7-T MRI may be useful for brain imaging, present 7-T protocols and sequences, and explore implementation challenges and potential solutions.

Unenhanced 7-T Brain MRI Protocol

Table 1 shows sequence parameters for our institutional routine 7-T unenhanced brain MRI protocol (acquisition time, approximately 25 minutes), which is modified from our 3-T unenhanced brain MRI protocol. A key sequence is a fat-saturated (FS) 3D T1-weighted MP-RAGE sequence with 0.3-mm isotropic images. This sequence affords detailed anatomic evaluation, including greater spatial resolution and contrast resolution for gray and white matter evaluation compared with acquisitions at lower field strengths [3], avoiding the need for a separate 2D T1-weighted turbo spin-echo (TSE) sequence. Owing to use of the local transmit head coil, the inflow of uninverted spins during acquisition with the sequence affords high vessel conspicuity, enabling reconstruction of MRA images (10-mm slice thickness, 1-mm interslice distance), also avoiding the need for a separate MRA acquisition [4–6]. This approach saves time in imaging of patients who need both brain MRI and brain MRA.

T2-weighted sequences include a 2-mm axial 2D FS FLAIR sequence and a 3-mm axial 2D FS T2-weighted TSE sequence. In our experience, 7-T FLAIR images are helpful but are not superior to 3-T FLAIR images. For example, gray-white matter differentiation is better on 3-T than on 7-T FLAIR images. Nonetheless, anatomic detail, SNR, and gray-white matter differentiation are better at 7 T compared with 3 T for 2D FS T2-weighted TSE sequences. In addition, DWI is acquired with a high-resolution readout segmentation of long variable echo trains (RESOLVE) sequence (three diffusion-sensitizing directions; maximal b value,

1000; slice thickness, 2 mm) [7]. A study showed that use of this sequence at 7 T compared with 1.5 or 3 T significantly improved detection of hippocampal abnormalities in patients with transient global amnesia [7]. The protocol also includes a susceptibility-weighted imaging (SWI) sequence. High sensitivity to magnetic susceptibility differences at 7 T improves detection of microhemorrhages, contusions, cavernomas, cerebral amyloidosis, and mineral deposits [8–11]. The strong susceptibility effects also allow excellent mapping of intracranial venous anatomy owing to the paramagnetic properties of deoxyhemoglobin in veins [12, 13]. A 2D T2*-weighted sequence may optionally be performed instead of both 2D FS T2-weighted TSE and SWI sequences. Figures 1 and 2 show examples.

Brain Tumors and Radiotherapy Planning

Use of 7-T MRI has numerous benefits for cranial tumor imaging. One significant advantage of 7 T is the ability to administer contrast media at half dose given increased T1 and T2* relaxivity [14–16]. At our center, all contrast-enhanced 7-T brain MRI examinations are performed at half dose (0.05 mL/kg) of contrast medium (gadobutrol, Gadavist, Bayer HealthCare). The improved SNR, CNR, and spatial resolution of 7-T MRI also improve delineation of the margins of tumor enhancement and of internal tumor components (e.g., neovascularization and internal necrosis) compared with MRI at lower field strengths [16, 17]. Improved susceptibility effects at 7 T aid visualization of intratumoral veins (Fig. 3A), microcalcifications, and microhemorrhages, and this may facilitate the determination that a tumor is likely high grade [12, 16–18]. Visualization of the elongation of corticomedullary vessels and displacement of medullary vessels with 7-T SWI may help differentiate oligodendrogliomas from astrocytomas [12]. The increased sensitivity of SWI at 7 T may also help detect microbleeds after radiotherapy [19].

Table 2 shows the 7-T brain tumor protocol (approximately 48 minutes) and the protocol for planning external beam radiotherapy after brain tumor surgery (approximately 30 minutes) used at our institution. Sequence parameters for the radiotherapy planning protocol differ slightly from those of the brain tumor protocol but are similar to the deep brain stimulator (DBS) planning protocol (see later, Parkinson Disease and Deep Brain Stimulator Placement). The brain tumor and radiotherapy protocols both include a sagittal 3D FLAIR SPACE sequence to evaluate the nonenhancing components of the tumors in three dimensions. The radiotherapy planning protocol includes an additional 3D T2-weighted SPACE sequence, which has lower spatial resolution but requires a shorter acquisition time and causes less artifact in the skull base. If perfusion imaging (see later, Dynamic Susceptibility Contrast Perfusion Imaging) is not performed, then DWI is acquired immediately after contrast medium injection before the contrast-enhanced 3D FS T1-weighted MP-RAGE sequence (Fig. 4).

Dynamic Susceptibility Contrast Perfusion Imaging

The brain tumor and radiotherapy planning protocols include an optional contrast-enhanced dynamic susceptibility contrast (DSC) perfusion sequence (provided by Siemens Healthineers application support) performed at the discretion of the ordering clinician and neuroradiologist. Although FDA-approved 7-T compatible power injectors are commercially

available, our institution does not have such a device. Thus, a half dose of contrast medium is administered by hand injection, without preloading, and followed by a saline flush. Acquisition with the DSC perfusion sequence is initiated 45 seconds before the start of contrast medium injection.

Using DSC perfusion data at 7 T, we have used two software packages (SyngoVIA, Siemens Healthineers; DynaSuite, MeVis Medical Solutions) to generate standard relative cerebral blood volume (rCBV), mean transit time, and relative cerebral blood flow maps; perfusion graphs; and quantitative measurements. The methods are the same as those used for such postprocessing at lower field strengths.

A benefit of 7 T for DSC perfusion imaging, in addition to the ability to use a lower dose of contrast medium, is greater resolution. At 3 T, the DSC sequence yields voxels measuring 1.7 × 1.7 mm in the axial plane with 5-mm slice thickness and 2-mm interslice distance. This low *z*-axis resolution at 3 T may lead to partial volume effects that confound interpretation of rCBV maps. Also, at 3 T, coronal reformatted rCBV maps used for fusion with anatomic images show significant staircase artifacts. In comparison, we obtain 7-T rCBV maps with a resolution of 1.5 × 1.5 × 1.6 mm. This higher resolution is beneficial for differentiating normal cortical perfusion from lesion perfusion and for differentiating tumor recurrence from radiation necrosis (Fig. 4). However, greater susceptibility artifacts may occur near the skull base at 7 T than at 3 T and cause a loss of perfusion information in this region on rCBV maps that limits assessment of normal structures and lesions (Fig. 4). Another limitation at 7 T is substantially longer postprocessing time (≈ 15–20 additional minutes) to generate the perfusion maps given the larger amount of data acquired.

Arterial spin labeling and blood oxygenation level–dependent 7-T perfusion techniques have also been described [20, 21], but we have not used these techniques clinically at our institution.

MR Spectroscopy

Compared with capabilities at 3 T, increased sensitivity and spectral resolution at 7 T substantially improve the precision of metabolite quantification and expand the potential to detect and reliably quantify weakly represented metabolites [22, 23]. The commercial 7-T scanner does not include built-in MR spectroscopy sequences. However, we have used an ultrashort-TE stimulated echo acquisition mode (STEAM) research sequence (Fig. 3) —previously validated in over 300 individuals [24–26]—for 7-T brain tumor imaging to evaluate metabolites that are difficult to quantify at lower field strengths and/or at long TE. Postprocessing and analysis require a separate workstation and dedicated software (Matlab, MathWorks, linear combination model [LC-Model], 2021) [24]. MR spectroscopy at 7 T has potential for better quantification of certain metabolites (e.g., 2-hydroxyglutarate and cystathionine) that are associated with brain tumor molecular markers (isocitrate dehydrogenase mutation and codeletion of chromosome arms 1p and 19q, respectively) [27–29].

Geometric Distortion

A known challenge in performing MRI for radiotherapy planning is related to geometric distortion (GD), the discrepancy between MRI appearance and actual anatomy [30]. Many factors contribute to GD, including hardware-related factors (e.g., magnetic field inhomogeneity, eddy currents, and gradient field non-linearity) and patient-related factors (e.g., susceptibility artifacts at the air-bone interface and chemical-shift effects) [30–32]. In a phantom study, GD was more severe at 7 T than at 3 T, particularly in the periphery of images and when the magnetization-prepared two rapid acquisition gradient echo (MP2RAGE) sequence was used [31]. GD measured less than 1 mm in the image center and thus could be ignored in this region; however, GD was greater for peripherally located lesions and thus should be recognized given the potential negative impact on dose calculations and radiotherapy targeting [31]. On the basis of our experience using a head phantom, we believe vendor-specific 3D distortion correction algorithms should be used to reduce GD. In addition, the use of interpolation during image acquisition increases GD. Finally, 7-T MRI might aid stereotactic planning for frameless procedures through the use of high receiver bandwidth sequences and properly calibrated gradients to achieve clinically acceptable error of less than 1.1 mm and with placement of specific skin-mounted fiducials in areas with minimal GD [32].

Multiple Sclerosis and Other Demyelinating Diseases

In patients with multiple sclerosis (MS), significantly more cortical or juxtacortical lesions are identified at 7 T than at 3 T in sequences such as 3D T1-weighted MP-RAGE, 3D FLAIR, and 3D dual inversion recovery [33–35]. This greater detection of cortical lesions may help differentiate MS from other demyelinating and white matter diseases (e.g., myelin oligodendrocyte glycoprotein antibody disease, neuromyelitis optica) that do not involve the cortex [36]. Nonetheless, a postmortem study showed that even 7-T MRI misses 40% of cortical lesions [34].

In patients with MS, the increased susceptibility effect at 7 T, in comparison with 3 T, improves visualization of the central vein sign (87% vs 45%) [37], which helps to differentiate MS from other white matter and demyelinating diseases [38]. For instance, in one study the sign was found in 60–80% of patients with MS versus 9% of patients with neuromyelitis optica [39].

Results of histopathologic investigations indicate that MS may cause meningeal inflammation and that 25% of patients with MS have meningeal inflammation on contrast-enhanced 3-T 3D FLAIR images [40]. In a small sample of patients with MS who underwent 7-T MRI with a 3D magnetization-prepared FLAIR sequence and image acquisition 20 minutes after contrast medium injection, 90% of patients had at least one enhancing leptomeningeal focus [41, 42]. However, this imaging finding is of unknown clinical significance, and its reporting is not recommended in current consensus guideline [43].

The 2021 consensus guideline on use of MRI in patients with MS does not recommend 7-T imaging [43], and a previously published 7-T brain MRI protocol for patients with MS lacks

information regarding the use of contrast media [44]. We, therefore, based our institutional 7-T protocol for MS and other demyelinating diseases, which takes approximately 54 minutes (Table 3), on the consensus guideline MS protocol for lower field strengths. The primary sequences in the protocol for detecting white matter and cortical lesions are 3D FLAIR SPACE and 3D dual inversion recovery SPACE. SWI and FS T2-weighted TSE are used to detect the central vein sign. The protocol also includes acquisition of a 3D FS T1-weighted MP-RAGE sequence before and after IV contrast medium administration to help identify enhancing lesions, hypointense foci, and subtle cortical lesions. Use of a half dose of contrast medium may be particularly advantageous in patients undergoing numerous routine follow-up examinations.

Clinical cervical and thoracic spine imaging at 7 T in patients with MS is currently impossible because of the absence of FDA-approved neck or spine coils for 7 T.

Parkinson Disease and Deep Brain Stimulator Placement

The “loss of swallowtail” sign is a promising MRI marker of Parkinson disease [11, 45]. The sign results from excess iron deposition in the pars compacta of the substantia nigra, causing susceptibility artifact and disappearance of the normal T2-hyperintense signal in the inner inferior and posterolateral part of the substantia nigra, which becomes hypointense on SWI [11, 45]. Detection of the loss of swallowtail sign can be challenging, especially in patients with Parkinson disease due to motion artifact resulting from tremors. At 7 T, however, a slightly oblique axial SWI or T2*-weighted acquisition in the orientation of the mesencephalon facilitates reliable assessment for the sign [45] (Fig. 5).

Use of 7 T can also aid DBS targeting, in which precise electrode placement in small subcortical structures (e.g., subthalamic nucleus, globus pallidus pars interna, ventral intermediate nucleus of the thalamus) is crucial for therapeutic efficacy. These structures are often difficult to visualize with conventional clinical sequences because of small size and central location. SWI and T2-weighted sequences with submillimeter resolution have been explored for reliably visualizing these structures and their borders at 7 T [46–50]. We acquire 2D T2-weighted TSE (0.4 × 0.4 × 1.0 mm) and localized 3D SWI slab (0.4 × 0.4 × 0.8 mm) images in axial and coronal orientations to generate patient-specific 3D anatomic models of the target structures and their surroundings. We use a combination of manual segmentation and artificial intelligence technology [47, 48, 51–54]. These models are used for planning of electrode implantation and, combined with postoperative CT images, help to determine the precise location of the DBS electrode relative to anatomic landmarks [47, 48]. The patient-specific postoperative model, accompanied by 7-T diffusion-based tractography and parcellation, also helps to explain clinical outcomes [54]. In one study, 7-T images used for presurgical planning showed minimal GD in the location of DBS targets that was similar in extent to GD observed at 1.5 T [49].

High-Detail Intracranial MRA, MR Venography, and Vessel Wall Imaging

MRA

Studies have shown that 7-T 3D time-of-flight (TOF) MRA and 3D MP-RAGE MRA techniques are superior to 1.5-T or 3-T 3D TOF MRA for characterization of intracranial aneurysms [5, 55–57]. For example, use of 7-T 3D TOF MRA changed the initial impression in 66% of patients in whom 3-T 3D TOF MRA was indeterminate regarding the presence of a true aneurysm versus prominent arterial infundibulum [57]. In another study, the combination of 3D TOF MRA and 3D MP-RAGE MRA at 7 T was comparable to reference-standard invasive digital subtraction angiography [58].

In our experience, 7-T 3D TOF MRA shows excellent detail of intracranial arteries and allows imaging of tiny perforating vessels (Fig. 6A). Limitations of 7-T 3D TOF MRA include poor imaging of the cavernous internal carotid arteries caused by susceptibility artifact and long acquisition time, which increases the likelihood of motion artifact. Anatomic coverage should be selected carefully to decrease acquisition time. Use of 3D MP-RAGE MRA may improve imaging of the petrous and cavernous internal carotid arteries with shorter acquisition times (Fig. 6B).

MR Venography

Our efforts to develop 7-T phase contrast and TOF MRV were unsuccessful because of an inability to properly saturate arterial flow at the skull base in healthy volunteers. However, we could obtain MRV images comparable to FLASH images shown in a prior case report [59] by subtracting precontrast 3D T1-weighted MP-RAGE images from postcontrast 3D T1-weighted MP-RAGE images (Fig. 7). This method may help delineate detailed venous anatomy and assist in the diagnosis of acute cerebral venous sinus thrombosis, but it may be limited in diagnosing enhancing subacute or chronic cerebral venous sinus thrombosis.

Vessel Wall Imaging

Use of 7 T is also promising for vessel wall imaging (VWI) Feng et al. [56] found better visualization of the aneurysm wall with 7-T VWI than with 3-T black-blood imaging. Another group [60–62] described 7-T VWI for evaluation of intracranial atherosclerosis. At our institution, 7-T VWI is used to evaluate for vasculitis and intracranial atherosclerosis. The protocol includes sagittal 3D FS T1-weighted SPACE with and without IV contrast medium for black-blood imaging, along with 3D TOF MRA (Fig. 8).

Pituitary Pathology

Despite more artifacts by the skull base, the improved resolution of 7-T MRI can be used to identify suspected pituitary microadenomas that were not visible at 1.5 T or 3 T. Small studies have shown better delineation of the margins of pituitary adenomas at 7 T [63–65]. In one study that included eight patients with Cushing disease and prior negative or equivocal 3-T MRI, 7-T MRI raised suspicion for pituitary microadenomas in all patients; postoperative pathologic analysis confirmed adenoma in seven patients [64]. An additional study that included 16 patients with biopsy-proven pituitary adenomas showed that 93.75%

of the adenomas were identified at 7 T versus 75.0% at 3 T and that 7 T afforded better lesion delineation [63]. The report of that study also described use of dynamic contrast-enhanced imaging for pituitary evaluation at 7 T. The 7-T pituitary protocol at our institution, which takes approximately 43 minutes (Table 4), includes sequences both with whole-brain anatomic coverage and with limited anatomic coverage of the pituitary gland and an optional dynamic contrast-enhanced T1-weighted FLASH acquisition. Figure 9 shows an example.

Epilepsy and Seizure

Approximately 20–30% of patients presenting with focal seizures have no identifiable lesion on 1.5-T or 3-T MRI [66]. Given increased SNR and higher spatial resolution, use of 7-T MRI may improve detection of subtle hippocampal abnormalities (e.g., early loss of hippocampal digitations, hippocampal malrotations), cortical malformations (e.g., heterotopia, polymicrogyria), subtle focal cortical dysplasia, and cavernomas [3, 8, 67–71]. The 7-T Epilepsy Task Force consensus report [68] recommends referral of patients with epilepsy to 7-T MRI for four indications: negative 3-T MRI; lesion typing, lesion delineation, and exclusion of false-positive lesions before surgical intervention; stealth guidance for electrode positioning; and identification of eloquent areas on functional MRI. This report also provides guidance for a 7-T epilepsy protocol, which is reflected in the epilepsy protocol at our institution, which takes approximately 55 minutes (Table 5). The protocol includes sequences with whole-brain anatomic coverage and limited anatomic coverage focused on the hippocampus. Because the consensus report does not provide information about use of contrast medium, contrast medium is used at the discretion of the referring clinician and the neuroradiologist.

When 7-T MRI is performed to evaluate for mesial temporal sclerosis, an oblique coronal 1.5-mm T2-weighted TSE sequence affords excellent detailed visualization of the hippocampi (Figs. 10A and 10B). However, 7-T skull base imaging with the currently available head coil is limited, and potential seizure foci in the inferior temporal gyri, such as encephaloceles and cortical abnormalities, may be obscured (Figs. 10C and 10D).

Challenges

Artifacts From B_1 Inhomogeneities and Magnetic Susceptibility

Transmit B_1 inhomogeneities (Fig. 11A) and susceptibility artifacts near the air-bone interface (Fig. 10D) limit the usefulness of 7-T MRI for assessment of structures near the skull base. Such artifacts at 7 T hinder evaluation of lower cranial nerve schwannomas, trigeminal neuralgia, abnormalities of internal auditory canal, inferior temporal lobe abnormalities, and osseous abnormalities of skull base [11, 68, 72, 73]. Interpreting radiologists may include a disclaimer in the report that such artifacts significantly impact image quality and lower sensitivity for skull base abnormalities. Dielectric pads are recommended to decrease these transmit B_1 inhomogeneities [68, 73] (Figs. 11B–11D). We use dielectric pads (either a commercially available pad [7TNS Neuro Set, Multiwave Imaging] or smaller pads made in-house with a 3:1 mass ratio of calcium titanate to water [74–76]) for all 7-T brain examinations unless these pads cannot fit within the head coil

owing to the size of the patient's head. When imaging the pituitary gland and hippocampus, we extend the patient's head within the coil as far as possible to shift the anatomy in the isocenter and decrease artifacts near the temporal bone, skull base, and sinuses.

Parallel transmission technology operates with multiple independent radiofrequency transmission channels to control the spatial distribution of the radiofrequency fields and improve the homogeneity of flip angle distribution. This method substantially reduces artifacts from B_1 inhomogeneity [77], which theoretically should become minimal. Additional benefits include more uniform image contrast, reduced specific absorption rate (SAR), and improved efficiency of image acquisition [78–80]. FDA-approved 7-T parallel transmission coils are expected to be available in the near future. Radiofrequency coils with extended sensitivity in the z-direction are also being explored to help reduce artifacts from B_1 inhomogeneity [81].

Artifacts From Motion, Pulsation, and Flow

The gains in SNR and CNR at 7 T do not necessarily translate into faster imaging. Typically, the gains in SNR are used to increase in-plane or through-plane spatial resolution. Although increased static magnetic fields support higher acceleration factors for parallel imaging [82], the desire for very high spatial resolution may in fact lead to longer acquisition times at 7 T, which in turn could accentuate artifacts from motion, pulsation, and flow (Fig. 2D).

Specific Absorption Rate

SAR increases with field strength and must be carefully controlled to ensure patient safety [83]. Because patient-specific SAR information is not available before an MRI examination, scanners rely on previous simulation results obtained from generic human models and on online power monitoring tools to determine safety levels. Additional radiofrequency safety factors are usually needed to ensure that SAR limits are not exceeded [84]. These measures may result in overly conservative operating conditions that limit scan efficiency. In general, SAR limits are more likely to be exceeded by sequences with large flip angles, short TR, and many slices (e.g., TSE and inversion recovery sequences and sequences with saturation band application). In our experience, SAR is a frequent limiting factor at 7 T. We typically perform clinical 7-T MRI using the scanner's first-level mode, which allows higher SAR limits compared with normal-level mode. For first-level mode, the International Electrotechnical Commission limits the peak 10-g–average local SAR to 20 W/kg, and the head-average SAR to 3.2 W/kg [85]. Strategies to reduce SAR include lengthening TR, decreasing flip angle, reducing the number of slices, and adjusting gradient modes. All such actions have trade-offs. For example, a longer TR may prolong acquisition time, in turn decreasing patient comfort and increasing motion artifact. The order of sequences may also be adjusted: for example, performing a low-SAR sequence between two high-SAR sequences. Additional radiofrequency coil design optimization concepts [81, 86, 87] and patient-specific SAR management strategies [88] have been described for addressing radiofrequency safety issues.

Patient Size and Weight

The commercially available 7-T scanner, in comparison with a current state-of-the-art 3-T system from the same vendor (Prisma, Siemens Healthineers) has the same bore diameter (60 cm) but a substantially greater bore length (270 vs 213 cm). Thus, for brain MRI at 7 T, the patient's entire body is enclosed within the scanner bore. This setup is less comfortable for patients and may lead to claustrophobia and motion artifact. For brain MRI examinations, we require that the patient's shoulder-to-shoulder width not exceed 58 cm; this limit may preclude performing brain MRI to evaluate for pituitary microadenoma in patients with Cushing syndrome. The commercially available 7-T scanner has a maximum allowed table weight of 200 kg [89]. Finally, the manufacturer's recommendations indicate that the scanner should not be used to image patients who weigh less than 30 kg, thereby limiting pediatric neuroimaging at 7 T [77, 89].

Metallic Hardware

Limited testing information is available from various vendors regarding the safety and compatibility of implanted hardware and devices for 7-T MRI. We therefore proceed cautiously with all implants. Each patient with an implant undergoes a preimaging assessment by the institution's MRI safety officer, who evaluates imaging parameters, imaging anatomy, implant location relative to the imaging anatomy, implant characteristics (including material and dimensions), and any available internal testing (i.e., performed onsite) or external testing (i.e., based on published literature) of the device or of similar devices. Using this process, we have performed 7-T MRI in patients with various metallic implants, including select titanium cranial hardware [90, 91], dental retainer wires [92], metallic dental materials (e.g., metals used for restoration, osseointegrated dental implants) [93], certain intrauterine devices [94], tattoos [94], and certain titanium spinal fixation hardware [91, 95]. We do not perform 7-T MRI in patients with large cranial meshes, aneurysm clips, cranial stents, or programmable ventriculoperitoneal shunt catheters.

For patients with metallic implants with minimal translational or rotational risk related to the static magnetic field and minimal peripheral nerve stimulation risk related to the gradient fields, there may still be persistent safety concern related to radiofrequency heating of the device. Nonetheless, 7-T MRI can still be feasible in these patients. For 7 T, in contrast to 1.5 and 3 T, the radiofrequency excitation is generally provided by local transmitter coils, for which electromagnetic fields rapidly decay outside of the sensitive region of the coil (corresponding to the imaged region). As a result, strong electromagnetic coupling does not occur for implants at a sufficient distance from the imaged anatomy. Therefore, in the absence of translational or rotational risk, 7-T MRI can typically be performed safely in the presence of a metallic implant located outside the sensitive region of the radiofrequency coil.

Side Effects

Dizziness, vertigo, nausea, headache, metallic taste, and peripheral nerve stimulation have been reported after 7-T MRI, although without associated serious adverse effect [96–99]. Dizziness and vertigo may occur as soon as the patient is brought into the scanner bore. In a study that included 577 individuals undergoing 7-T MRI, 60.4% reported dizziness and vertigo, which were experienced particularly during table movement, and 0.7% needed to

abort the MRI when positioned in the unit [99]. To avoid dizziness, the patient should move slowly when being positioned on the table; the table should be moved slowly into the bore; and the patient should keep their head directly in the midline or close their eyes while the table moves in or out of the bore. At the conclusion of the examination, patients should likewise sit up slowly to avoid orthostatic hypotension. If dizziness occurs, the patient should wait for a minute or two on the table until the dizziness resolves. In our experience, through such measures, an aborted examination due to dizziness or vertigo at the beginning of the study is extremely rare.

One study showed metallic taste after 7-T MRI in 11% of patients [98]. However, we have not received a report of metallic taste after 7-T MRI from a single patient.

The noise level is reported to be similar between 3-T and 7-T MRI [76]. In our experience, the noise level at 7 T is similar to that encountered in a 3-T Prisma system. However, the available head coil for 7-T MRI is smaller at than that used at 3 T, limiting the use of noise-canceling headphones.

Future Direction and Goals

Routine clinical brain imaging with 7-T MRI is in its early stages. Clinical implementation of parallel transmission systems would be a crucial advance in mitigating shortcomings of the current single-channel transmit system. Additional future improvements include development of an FDA-approved integrated head and neck coil, vendor-supplied MR spectroscopy sequences, and patient-specific implant safety assessment protocols. Investigation of the safety of 7-T MRI in children is also warranted. Finally, further research should seek to establish the added usefulness of 7-T brain MRI for specific clinical indications with focus on potentially improved patient outcomes.

Acknowledgment

We thank Pierre-François Van de Moortele (University of Minnesota), who made significant contributions to this work before he died in 2022.

References

1. U.S. Food and Drug Administration website. FDA clears first 7T magnetic resonance imaging device. www.fda.gov/news-events/press-announcements/fda-clears-first-7t-magnetic-resonance-imaging-device. Published Oct 12, 2017. Accessed Jun 8, 2023
2. Ugurbil K Magnetic resonance imaging at ultrahigh fields. IEEE Trans Biomed Eng 2014; 61:1364–1379 [PubMed: 24686229]
3. Zampeli A, Hansson B, Bloch KM, et al. Structural association between heterotopia and cortical lesions visualised with 7 T MRI in patients with focal epilepsy. Seizure 2022; 101:177–183 [PubMed: 36058100]
4. Madai VI, von Samson–Himmelstjerna FC, Sandow N, et al. Ultrahigh-field MPRAGE magnetic resonance angiography at 7.0 T in patients with cerebrovascular disease. Eur J Radiol 2015; 84:2613–2617 [PubMed: 26462794]
5. Wrede KH, Dammann P, Mönninghoff C, et al. Non-enhanced MR imaging of cerebral aneurysms: 7 Tesla versus 1.5 Tesla. PLoS One 2014; 9:e84562 [PubMed: 24400100]

6. Grinstead JW, Rooney W, Laub G. The origins of bright blood MPRAGE at 7 Tesla and a simultaneous method for T1 imaging and non-contrast MRA. Proc Intl Soc Magn Reson Med 2010; 18:1429
7. Unsgård RG, Doan TP, Nordlid KK, Kvistad KA, Goa PE, Berntsen EM. Transient global amnesia: 7 Tesla MRI reveals more hippocampal lesions with diffusion restriction compared to 1.5 and 3 Tesla MRI. Neuroradiology 2022; 64:2217–2226 [PubMed: 35754063]
8. Dammann P, Barth M, Zhu Y, et al. Susceptibility weighted magnetic resonance imaging of cerebral cavernous malformations: prospects, drawbacks, and first experience at ultra-high field strength (7-Tesla) magnetic resonance imaging. Neurosurg Focus 2010; 29:E5
9. van Harten TW, Heijmans A, van Rooden S, et al. Brain deep medullary veins on 7T MRI in Dutch-type hereditary cerebral amyloid angiopathy. J Alzheimers Dis 2022; 90:381–388 [PubMed: 36120778]
10. Koemans EA, van Etten ES, van Opstal AM, et al. Innovative magnetic resonance imaging markers of hereditary cerebral amyloid angiopathy at 7 Tesla. Stroke 2018; 49:1518–1520 [PubMed: 29695466]
11. Okada T, Fujimoto K, Fushimi Y, et al. Neuroimaging at 7 Tesla: a pictorial narrative review. Quant Imaging Med Surg 2022; 12:3406–3435 [PubMed: 35655840]
12. Natsumeda M, Matsuzawa H, Watanabe M, et al. SWI by 7T MR imaging for the microscopic imaging diagnosis of astrocytic and oligodendroglial tumors. AJNR 2022; 43:1575–1581 [PubMed: 36229164]
13. Frischer JM, Göd S, Gruber A, et al. Susceptibility-weighted imaging at 7 T: improved diagnosis of cerebral cavernous malformations and associated developmental venous anomalies. Neuroimage Clin 2012; 1:116–120 [PubMed: 24179744]
14. Noebauer-Huhmann IM, Szomolanyi P, Kronnerwetter C, et al. Brain tumours at 7T MRI compared to 3T: contrast effect after half and full standard contrast agent dose: initial results. Eur Radiol 2015; 25:106–112 [PubMed: 25194707]
15. Kalavagunta C, Michaeli S, Metzger GJ. In vitro Gd-DTPA relaxometry studies in oxygenated venous human blood and aqueous solution at 3 and 7 T. Contrast Media Mol Imaging 2014; 9:169–176 [PubMed: 24523062]
16. Morrison MA, Lupo JM. 7-T magnetic resonance imaging in the management of brain tumors. Magn Reson Imaging Clin N Am 2021; 29:83–102 [PubMed: 33237018]
17. Paek SL, Chung YS, Paek SH, et al. Early experience of pre- and post-contrast 7.0T MRI in brain tumors. J Korean Med Sci 2013; 28:1362–1372 [PubMed: 24015044]
18. Shaffer A, Kwok SS, Naik A, et al. Ultra-high-field MRI in the diagnosis and management of gliomas: a systematic review. Front Neurol 2022; 13:857825 [PubMed: 35449515]
19. Morrison MA, Mueller S, Felton E, et al. Rate of radiation-induced microbleed formation on 7T MRI relates to cognitive impairment in young patients treated with radiation therapy for a brain tumor. Radiother Oncol 2021; 154:145–153 [PubMed: 32966846]
20. Harteveld AA, van der Kolk AG, Zwanenburg JJ, Luijten PR, Hendrikse J. 7-T MRI in cerebrovascular diseases: challenges to overcome and initial results. Top Magn Reson Imaging 2016; 25:89–100 [PubMed: 27049246]
21. Pfeuffer J, Adriany G, Shmuel A, et al. Perfusion-based high-resolution functional imaging in the human brain at 7 Tesla. Magn Reson Med 2002; 47:903–911 [PubMed: 11979569]
22. Terpstra M, Cheong I, Lyu T, et al. Test-retest reproducibility of neurochemical profiles with short-echo, single-voxel MR spectroscopy at 3T and 7T. Magn Reson Med 2016; 76:1083–1091 [PubMed: 26502373]
23. Deelchand DK, Iltis I, Henry PG. Improved quantification precision of human brain short echo-time (1)H magnetic resonance spectroscopy at high magnetic field: a simulation study. Magn Reson Med 2014; 72:20–25 [PubMed: 23900976]
24. Marjańska M, McCarten JR, Hodges J, et al. Region-specific aging of the human brain as evidenced by neurochemical profiles measured noninvasively in the posterior cingulate cortex and the occipital lobe using ^{1}H magnetic resonance spectroscopy at 7 T. Neuroscience 2017; 354:168–177 [PubMed: 28476320]

25. Schallmo MP, Weldon KB, Kamath RS, et al. The psychosis human connectome project: design and rationale for studies of visual neurophysiology. Neuroimage 2023; 272:120060 [PubMed: 36997137]
26. University of Minnesota website. CMRR spectroscopy package. www.cmrr.umn.edu/spectro. Latest release Aug 2022. Accessed May 15, 2023
27. Andronesi OC, Kim GS, Gerstner E, et al. Detection of 2-hydroxyglutarate in IDH-mutated glioma patients by in vivo spectral-editing and 2D correlation magnetic resonance spectroscopy. Sci Transl Med 2012; 4:116ra4
28. Choi C, Ganji SK, DeBerardinis RJ, et al. 2-Hydroxyglutarate detection by magnetic resonance spectroscopy in IDH-mutated patients with gliomas. Nat Med 2012; 18:624–629 [PubMed: 22281806]
29. Branzoli F, Pontoizeau C, Tchara L, et al. Cystathionine as a marker for 1p/19q codeleted gliomas by in vivo magnetic resonance spectroscopy. Neuro Oncol 2019; 21:765–774 [PubMed: 30726924]
30. Weygand J, Fuller CD, Ibbott GS, et al. Spatial precision in magnetic resonance imaging-guided radiation therapy: the role of geometric distortion. Int J Radiat Oncol Biol Phys 2016; 95:1304–1316 [PubMed: 27354136]
31. Peerlings J, Compter I, Janssen F, et al. Characterizing geometrical accuracy in clinically optimised 7T and 3T magnetic resonance images for high-precision radiation treatment of brain tumours. Phys Imaging Radiat Oncol 2019; 9:35–42 [PubMed: 33458423]
32. Kirby KM, Koons EK, Welker KM, Fagan AJ. Minimizing magnetic resonance image geometric distortion at 7 Tesla for frameless presurgical planning using skin-adhered fiducials. Med Phys 2023; 50:694–701 [PubMed: 36301228]
33. de Graaf WL, Kilsdonk ID, Lopez-Soriano A, et al. Clinical application of multi-contrast 7-T MR imaging in multiple sclerosis: increased lesion detection compared to 3 T confined to grey matter. Eur Radiol 2013; 23:528–540 [PubMed: 22898935]
34. Kilsdonk ID, Jonkman LE, Klaver R, et al. Increased cortical grey matter lesion detection in multiple sclerosis with 7 T MRI: a post-mortem verification study. Brain 2016; 139:1472–1481 [PubMed: 26956422]
35. Tallantyre EC, Morgan PS, Dixon JE, et al. 3 Tesla and 7 Tesla MRI of multiple sclerosis cortical lesions. J Magn Reson Imaging 2010; 32:971–977 [PubMed: 20882628]
36. Cortese R, Prados Carrasco F, Tur C, et al. Differentiating multiple sclerosis from AQP4-neuromyelitis optica spectrum disorder and MOG-antibody disease with imaging. Neurology 2023; 100:e308–e323 [PubMed: 36192175]
37. Tallantyre EC, Morgan PS, Dixon JE, et al. A comparison of 3T and 7T in the detection of small parenchymal veins within MS lesions. Invest Radiol 2009; 44:491–494
38. Bruschi N, Boffa G, Inglese M. Ultra-high-field 7-T MRI in multiple sclerosis and other demyelinating diseases: from pathology to clinical practice. Eur Radiol Exp 2020; 4:59 [PubMed: 33089380]
39. Kister I, Herbert J, Zhou Y, Ge Y. Ultrahigh-field MR (7 T) imaging of brain lesions in neuromyelitis optica. Mult Scler Int 2013; 2013:398259 [PubMed: 23431447]
40. Absinta M, Vuolo L, Rao A, et al. Gadolinium-based MRI characterization of leptomeningeal inflammation in multiple sclerosis. Neurology 2015; 85:18–28 [PubMed: 25888557]
41. Harrison DM, Wang KY, Fiol J, et al. Leptomeningeal enhancement at 7T in multiple sclerosis: frequency, morphology, and relationship to cortical volume. J Neuroimaging 2017; 27:461–468 [PubMed: 28464368]
42. Jonas SN, Izbudak I, Frazier AA, Harrison DM. Longitudinal persistence of meningeal enhancement on postcontrast 7T 3D-FLAIR MRI in multiple sclerosis. AJNR 2018; 39:1799–1805 [PubMed: 30213813]
43. Wattjes MP, Ciccarelli O, Reich DS, et al. ; Magnetic Resonance Imaging in Multiple Sclerosis Study Group, Consortium of Multiple Sclerosis Centres, North American Imaging in Multiple Sclerosis Cooperative Guidelines Working Group. 2021 MAGNIMS-CMSC-NAIMS consensus recommendations on the use of MRI in patients with multiple sclerosis. Lancet Neurol 2021; 20:653–670 [PubMed: 34139157]

44. Cocozza S, Cosottini M, Signori A, et al. A clinically feasible 7-Tesla protocol for the identification of cortical lesions in multiple sclerosis. Eur Radiol 2020; 30:4586–4594 [PubMed: 32211962]
45. Schmidt MA, Engelhorn T, Marxreiter F, et al. Ultra high-field SWI of the substantia nigra at 7T: reliability and consistency of the swallow-tail sign. BMC Neurol 2017; 17:194 [PubMed: 29073886]
46. Abosch A, Yacoub E, Ugurbil K, Harel N. An assessment of current brain targets for deep brain stimulation surgery with susceptibility-weighted imaging at 7 tesla. Neurosurgery 2010; 67:1745–1756; discussion, 1756 [PubMed: 21107206]
47. Duchin Y, Shamir RR, Patriat R, et al. Patient-specific anatomical model for deep brain stimulation based on 7 Tesla MRI. PLoS One 2018; 13:e0201469 [PubMed: 30133472]
48. Patriat R, Cooper SE, Duchin Y, et al. Individualized tractography-based parcellation of the globus pallidus pars interna using 7T MRI in movement disorder patients prior to DBS surgery. Neuroimage 2018; 178:198–209 [PubMed: 29787868]
49. Duchin Y, Abosch A, Yacoub E, Sapiro G, Harel N. Feasibility of using ultra-high field (7 T) MRI for clinical surgical targeting. PLoS One 2012; 7:e37328 [PubMed: 22615980]
50. Plantinga BR, Temel Y, Duchin Y, et al. Individualized parcellation of the subthalamic nucleus in patients with Parkinson's disease with 7T MRI. Neuroimage 2018; 168:403–411 [PubMed: 27688203]
51. Solomon O, Palnitkar T, Patriat R, et al. Deep-learning based fully automatic segmentation of the globus pallidus interna and externa using ultra-high 7 Tesla MRI. Hum Brain Mapp 2021; 42:2862–2879 [PubMed: 33738898]
52. Shamir RR, Duchin Y, Kim J, et al. Microelectrode recordings validate the clinical visualization of subthalamic-nucleus based on 7T magnetic resonance imaging and machine learning for deep brain stimulation surgery. Neurosurgery 2019; 84:749–757 [PubMed: 29800386]
53. Kim J, Duchin Y, Shamir RR, et al. Automatic localization of the subthalamic nucleus on patient-specific clinical MRI by incorporating 7 T MRI and machine learning: application in deep brain stimulation. Hum Brain Mapp 2019; 40:679–698 [PubMed: 30379376]
54. Schrock LE, Patriat R, Goftari M, et al. 7T MRI and computational modeling supports a critical role of lead location in determining outcomes for deep brain stimulation: a case report. Front Hum Neurosci 2021; 15:631778 [PubMed: 33679351]
55. De Cocker LJ, Lindenholz A, Zwanenburg JJ, et al. Clinical vascular imaging in the brain at 7T. Neuroimage 2018; 168:452–458 [PubMed: 27867089]
56. Feng J, Liu X, Zhang Z, et al. Comparison of 7 T and 3 T vessel wall MRI for the evaluation of intracranial aneurysm wall. Eur Radiol 2022; 32:2384–2392 [PubMed: 34643780]
57. Radojewski P, Slotboom J, Joseph A, Wiest R, Mordasini P. Clinical implementation of 7T MRI for the identification of incidental intracranial aneurysms versus anatomic variants. AJNR 2021; 42:2172–2174 [PubMed: 34711553]
58. Wrede KH, Matsushige T, Goericke SL, et al. Non-enhanced magnetic resonance imaging of unruptured intracranial aneurysms at 7 Tesla: comparison with digital subtraction angiography. Eur Radiol 2017; 27:354–364 [PubMed: 26993650]
59. Lakhani DA, Middlebrooks EH. MR intracranial venography at 7 T. Radiology 2022; 304:529 [PubMed: 35536135]
60. Harteveld AA, van der Kolk AG, van der Worp HB, et al. High-resolution intracranial vessel wall MRI in an elderly asymptomatic population: comparison of 3T and 7T. Eur Radiol 2017; 27:1585–1595 [PubMed: 27387876]
61. Lindenholz A, van der Kolk AG, Zwanenburg JJM, Hendrikse J. The use and pitfalls of intracranial vessel wall imaging: how we do it. Radiology 2018; 286:12–28 [PubMed: 29261469]
62. van der Kolk AG, Zwanenburg JJ, Denswil NP, et al. Imaging the intracranial atherosclerotic vessel wall using 7T MRI: initial comparison with histopathology. AJNR 2015; 36:694–701 [PubMed: 25477359]
63. Eisenhut F, Schlaffer SM, Hock S, et al. Ultra-high-field 7 T magnetic resonance imaging including dynamic and static contrast-enhanced T1-weighted imaging improves detection of secreting pituitary microadenomas. Invest Radiol 2022; 57:567–574 [PubMed: 35925660]

64. Patel V, Liu CJ, Shiroishi MS, et al. Ultra-high field magnetic resonance imaging for localization of corticotropin-secreting pituitary adenomas. Neuroradiology 2020; 62:1051–1054 [PubMed: 32306052]

65. Rutland JW, Delman BN, Feldman RE, et al. Utility of 7 Tesla MRI for preoperative planning of endoscopic endonasal surgery for pituitary adenomas. J Neurol Surg B Skull Base 2021; 82:303–312 [PubMed: 34026406]

66. Winston GP, Micallef C, Kendell BE, et al. The value of repeat neuroimaging for epilepsy at a tertiary referral centre: 16 years of experience. Epilepsy Res 2013; 105:349–355 [PubMed: 23538269]

67. Park JE, Cheong EN, Jung DE, Shim WH, Lee JS. Utility of 7 Tesla magnetic resonance imaging in patients with epilepsy: a systematic review and meta-analysis. Front Neurol 2021; 12:621936 [PubMed: 33815251]

68. Opheim G, van der Kolk A, Markenroth Bloch K, et al. 7T Epilepsy Task Force consensus recommendations on the use of 7T MRI in clinical practice. Neurology 2021; 96:327–341 [PubMed: 33361257]

69. Henry TR, Chupin M, Lehéricy S, et al. Hippocampal sclerosis in temporal lobe epilepsy: findings at 7 T. Radiology 2011; 261:199–209 [PubMed: 21746814]

70. Colon AJ, van Osch MJ, Buijs M, et al. Detection superiority of 7 T MRI protocol in patients with epilepsy and suspected focal cortical dysplasia. Acta Neurol Belg 2016; 116:259–269 [PubMed: 27389578]

71. De Ciantis A, Barkovich AJ, Cosottini M, et al. Ultra-high-field MR imaging in polymicrogyria and epilepsy. AJNR 2015; 36:309–316 [PubMed: 25258368]

72. Ma R, Henry TR, Van de Moortele PF. Eliminating susceptibility induced hyperintensities in T1W MPRAGE brain images at 7 T. Magn Reson Imaging 2019; 63:274–279 [PubMed: 31446038]

73. Yang QX, Mao W, Wang J, et al. Manipulation of image intensity distribution at 7.0 T: passive RF shimming and focusing with dielectric materials. J Magn Reson Imaging 2006; 24:197–202 [PubMed: 16755543]

74. Teeuwisse WM, Brink WM, Webb AG. Quantitative assessment of the effects of high-permittivity pads in 7 Tesla MRI of the brain. Magn Reson Med 2012; 67:1285–1293 [PubMed: 21826732]

75. Snaar JE, Teeuwisse WM, Versluis MJ, et al. Improvements in high-field localized MRS of the medial temporal lobe in humans using new deformable high-dielectric materials. NMR Biomed 2011; 24:873–879 [PubMed: 21834010]

76. Fagan AJ, Bitz AK, Björkman-Burtscher IM, Collins CM, Kimbrell V, Raaijmak-ers AJE; ISMRM Safety Committee. 7T MR Safety. J Magn Reson Imaging 2021; 53:333–346 [PubMed: 32830900]

77. Padormo F, Beqiri A, Hajnal JV, Malik SJ. Parallel transmission for ultrahigh-field imaging. NMR Biomed 2016; 29:1145–1161 [PubMed: 25989904]

78. Wu X, Auerbach EJ, Vu AT, et al. High-resolution whole-brain diffusion MRI at 7T using radiofrequency parallel transmission. Magn Reson Med 2018; 80:1857–1870 [PubMed: 29603381]

79. Sharma A, Bammer R, Stenger VA, Grissom WA. Low peak power multiband spokes pulses for B1 (+) inhomogeneity-compensated simultaneous multislice excitation in high field MRI. Magn Reson Med 2015; 74:747–755 [PubMed: 25203620]

80. Beqiri A, Hoogduin H, Sbrizzi A, Hajnal JV, Malik SJ. Whole-brain 3D FLAIR at 7T using direct signal control. Magn Reson Med 2018; 80:1533–1545 [PubMed: 29476551]

81. May MW, Hansen SJD, Mahmutovic M, et al. A patient-friendly 16-channel transmit/64-channel receive coil array for combined head-neck MRI at 7 Tesla. Magn Reson Med 2022; 88:1419–1433 [PubMed: 35605167]

82. Wiesinger F, Van de Moortele PF, Adriany G, De Zanche N, Ugurbil K, Pruessmann KP. Parallel imaging performance as a function of field strength: an experimental investigation using electrodynamic scaling. Magn Reson Med 2004; 52:953–964 [PubMed: 15508167]

83. Collins CM, Wang Z. Calculation of radiofrequency electromagnetic fields and their effects in MRI of human subjects. Magn Reson Med 2011; 65:1470–1482 [PubMed: 21381106]

84. Steensma BR, Sadeghi-Tarakameh A, Meliadò EF, et al. Tier-based formalism for safety assessment of custom-built radio-frequency transmit coils. NMR Biomed 2023; 36:e4874 [PubMed: 36368912]

85. International Electrotechnical Commission. IEC 60601–2-33:2022: medical electrical equipment. Part 2–33. Particular requirements for the basic safety and essential performance of magnetic resonance equipment for medical diagnosis. In: International standard, 4th ed. International Electrotechnical Commission, 2022
86. Avdievich NI, Nikulin AV, Ruhm L, et al. A 32-element loop/dipole hybrid array for human head imaging at 7 T. Magn Reson Med 2022; 88:1912–1926 [PubMed: 35766426]
87. Sadeghi-Tarakameh A, Jungst S, Lanagan M, et al. A nine-channel transmit/receive array for spine imaging at 10.5 T: introduction to a nonuniform dielectric substrate antenna. Magn Reson Med 2022; 87:2074–2088 [PubMed: 34825735]
88. Brink WM, Yousefi S, Bhatnagar P, Remis RF, Staring M, Webb AG. Personalized local SAR prediction for parallel transmit neuroimaging at 7T from a single T1-weighted dataset. Magn Reson Med 2022; 88:464–475 [PubMed: 35344602]
89. Siemens Healthineers website. Datasheet: Magnetom Terra. marketing. webassets.siemens-healthineers.com/1800000007484744/4402e89c070d/MR-MAGNETOM-Terra_Datasheet_USA_1800000007484744.pdf. Published Aug 2020. Accessed Mar 18, 2023
90. Chen B, Schoemberg T, Kraff O, et al. Cranial fixation plates in cerebral magnetic resonance imaging: a 3 and 7 Tesla in vivo image quality study. MAGMA 2016; 29:389–398 [PubMed: 27026243]
91. Shaffer A, Weisbaum D, Naik A, et al. Neurosurgical implant safety in 7 T MRI: a scoping review. J Magn Reson Imaging 2023; 57:661–669 [PubMed: 36173367]
92. Wezel J, Kooij BJ, Webb AG. Assessing the MR compatibility of dental retainer wires at 7 Tesla. Magn Reson Med 2014; 72:1191–1198 [PubMed: 24408149]
93. Oriso K, Kobayashi T, Sasaki M, Uwano I, Kihara H, Kondo H. Impact of the static and radiofrequency magnetic fields produced by a 7T MR imager on metallic dental materials. Magn Reson Med Sci 2016; 15:26–330 [PubMed: 25994037]
94. Noureddine Y, Bitz AK, Ladd ME, et al. Experience with magnetic resonance imaging of human subjects with passive implants and tattoos at 7 T: a retrospective study. MAGMA 2015; 28:577–590 [PubMed: 26410044]
95. Tsukimura I, Murakami H, Sasaki M, et al. Assessment of magnetic field interactions and radiofrequency-radiation-induced heating of metallic spinal implants in 7 T field. J Orthop Res 2017; 35:1831–1837 [PubMed: 27769107]
96. Theysohn JM, Maderwald S, Kraff O, Moenninghoff C, Ladd ME, Ladd SC. Subjective acceptance of 7 Tesla MRI for human imaging. MAGMA 2008; 21:63–72 [PubMed: 18064501]
97. Cosottini M, Frosini D, Biagi L, et al. Short-term side-effects of brain MR examination at 7 T: a single-centre experience. Eur Radiol 2014; 24:1923–1928 [PubMed: 24816933]
98. Versluis MJ, Teeuwisse WM, Kan HE, van Buchem MA, Webb AG, van Osch MJ. Subject tolerance of 7 T MRI examinations. J Magn Reson Imaging 2013; 38:722–725 [PubMed: 23150466]
99. Heilmaier C, Theysohn JM, Maderwald S, Kraff O, Ladd ME, Ladd SC. A large-scale study on subjective perception of discomfort during 7 and 1.5 T MRI examinations. Bioelectromagnetics 2011; 32:610–619 [PubMed: 21598286]

Highlights

- This article describes clinical indications where 7-T MRI may be useful for brain imaging, presents 7-T protocols and sequences, and explores challenges and potential solutions.

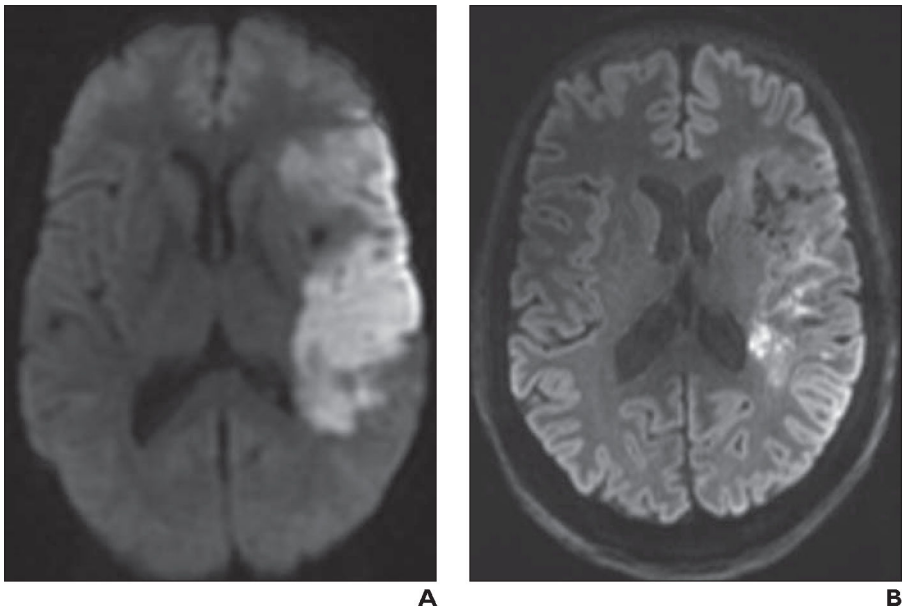

Fig. 1—.

62-year-old woman who presented with right-sided acute stroke.

A, Initial axial 1.5-T DWI obtained at 5-mm slice thickness shows acute left middle cerebral artery infarct.

B, Axial 7-T readout segmentation of long variable echo trains (RESOLVE) DWI at 2-mm slice thickness obtained 11 days after **A** shows expected resolution of infarct, which is now subacute. Image at 7 T exhibits markedly improved spatial resolution and contrast resolution compared with 1.5-T image.

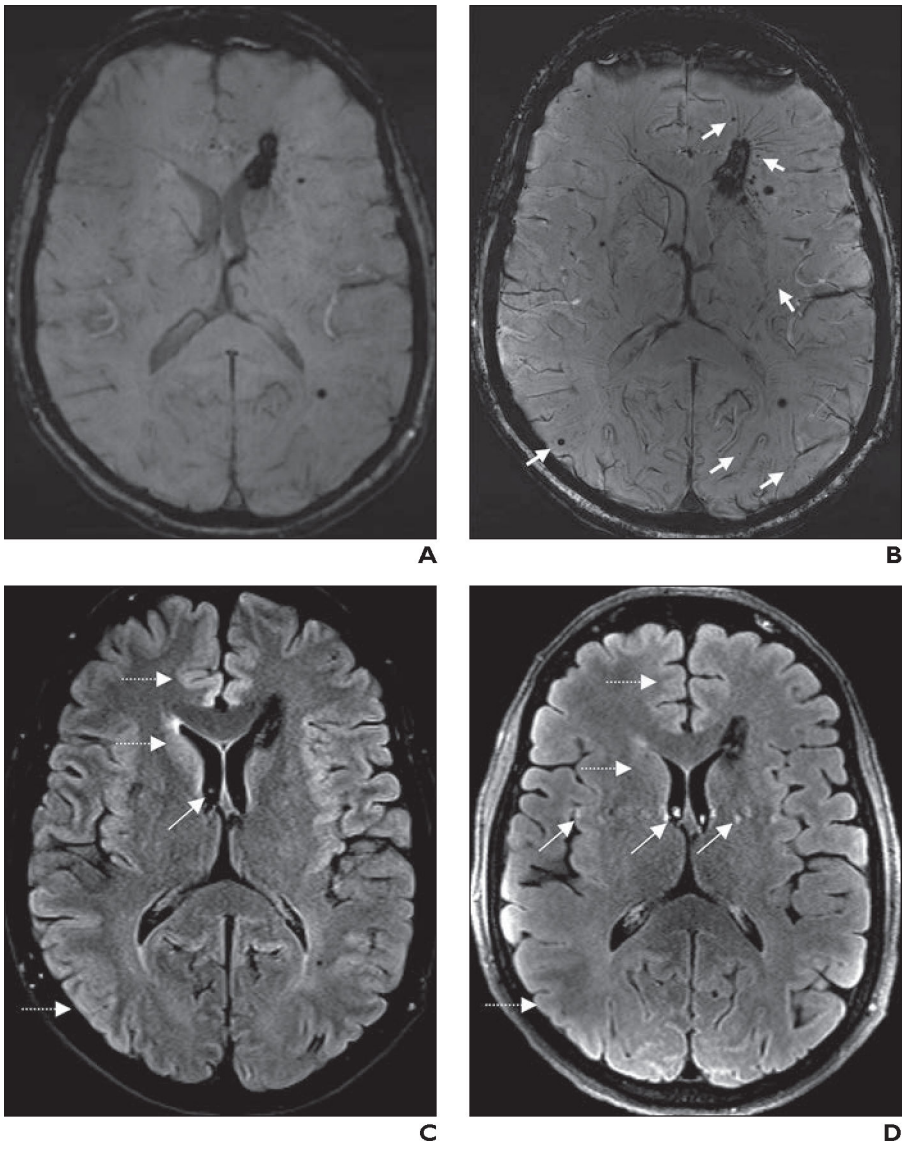

Fig. 2—.

56-year-old man with known multiple cerebral cavernomas.

A, Axial 3-T susceptibility-weighted imaging (SWI) shows cavernomas, which are stable compared with appearance on prior surveillance MRI examinations performed over many years.

B, Axial 7-T SWI obtained 18 months after **A** shows additional tiny cavernomas (*arrows*), which were not visible at 3 T, and greater conspicuity of draining veins associated with largest periventricular cavernoma.

C, Axial 2D 3-T fat-saturated FLAIR image from same examination as **A** shows subtle CSF pulsation artifacts (*oblique arrow*). Gray-white matter differentiation (*horizontal arrows*) in frontal lobes, basal ganglia, temporal lobes, and insular cortexes is better than at 7 T.

D, Axial 2D 7-T fat-saturated FLAIR image from same examination as **B** shows more pronounced CSF pulsation artifacts (*oblique arrows*). Gray-white matter differentiation

(*horizontal arrows*) in frontal lobes, basal ganglia, temporal lobes, and insular cortexes is worse than at 3 T.

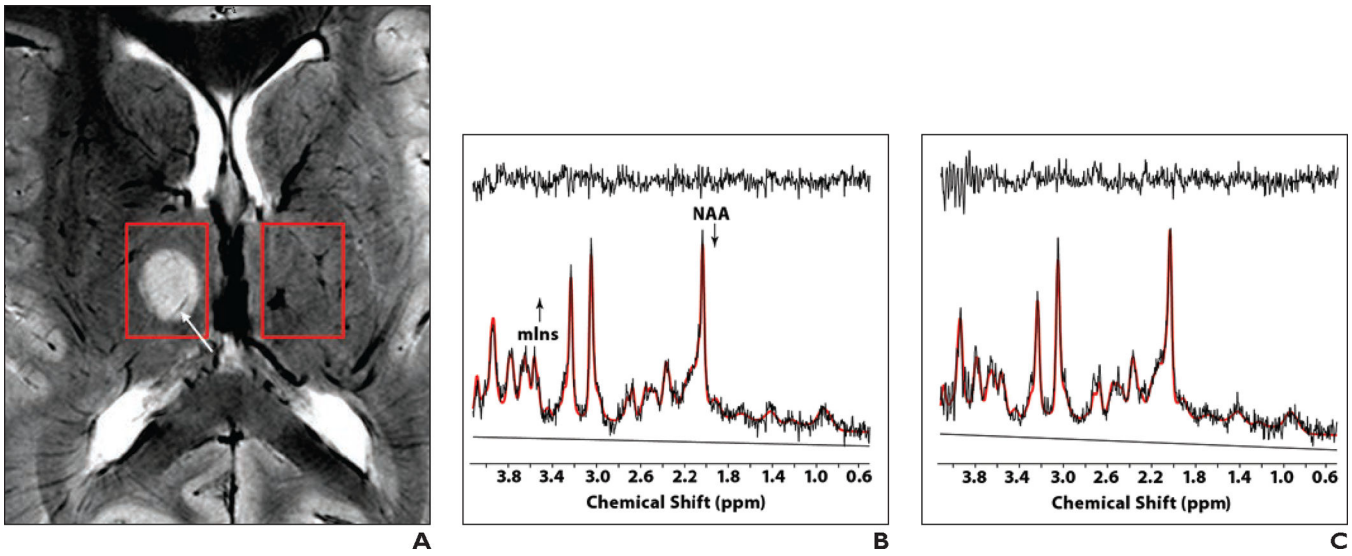

Fig. 3—.

12-year-old girl with incidental right thalamic mass found on imaging performed at outside institution. Patient was referred for 7-T MRI, including MR spectroscopy.

A, Unenhanced T2*-weighted MR image shows well-circumscribed T2-hyperintense homogeneous lesion in right thalamus. Intratumoral venous architecture (*arrow*), which was not visible on prior 3-T examination (not shown), is evident. Lesion did not exhibit enhancement on additional contrast-enhanced images (not shown). Boxes denote lesion (*left*) and contralateral portion of brain (*right*) used for spectra in **B** and **C**.

B and **C,** Spectra obtained with 7-T ultrashort-TE stimulated echo acquisition mode (STEAM) sequence (TR/TE, 3/8; mixing time, 32 ms; 64 shots; volume, 17 × 13 × 17 mm) show results for lesion (**B**; *right box*, **A**) and contralateral portion of brain (**C**; *left box*, **A**). Plots show in vivo spectra, linear combination model (LCModel) fits (*red*), residuals (*top tracing*), and baseline contributions (*bottom tracing*). No line broadening is applied to spectra. Both spectra are of good quality and have different appearance from spectra obtained at lower field strength or with longer TE. Analysis showed lower *N*-acetyl aspartate (NAA) level and higher myo-inositol (mIns) level in thalamus lesion than in contralateral region. Constellation of MRI and MR spectroscopy findings indicate that lesion is low-grade glioma.

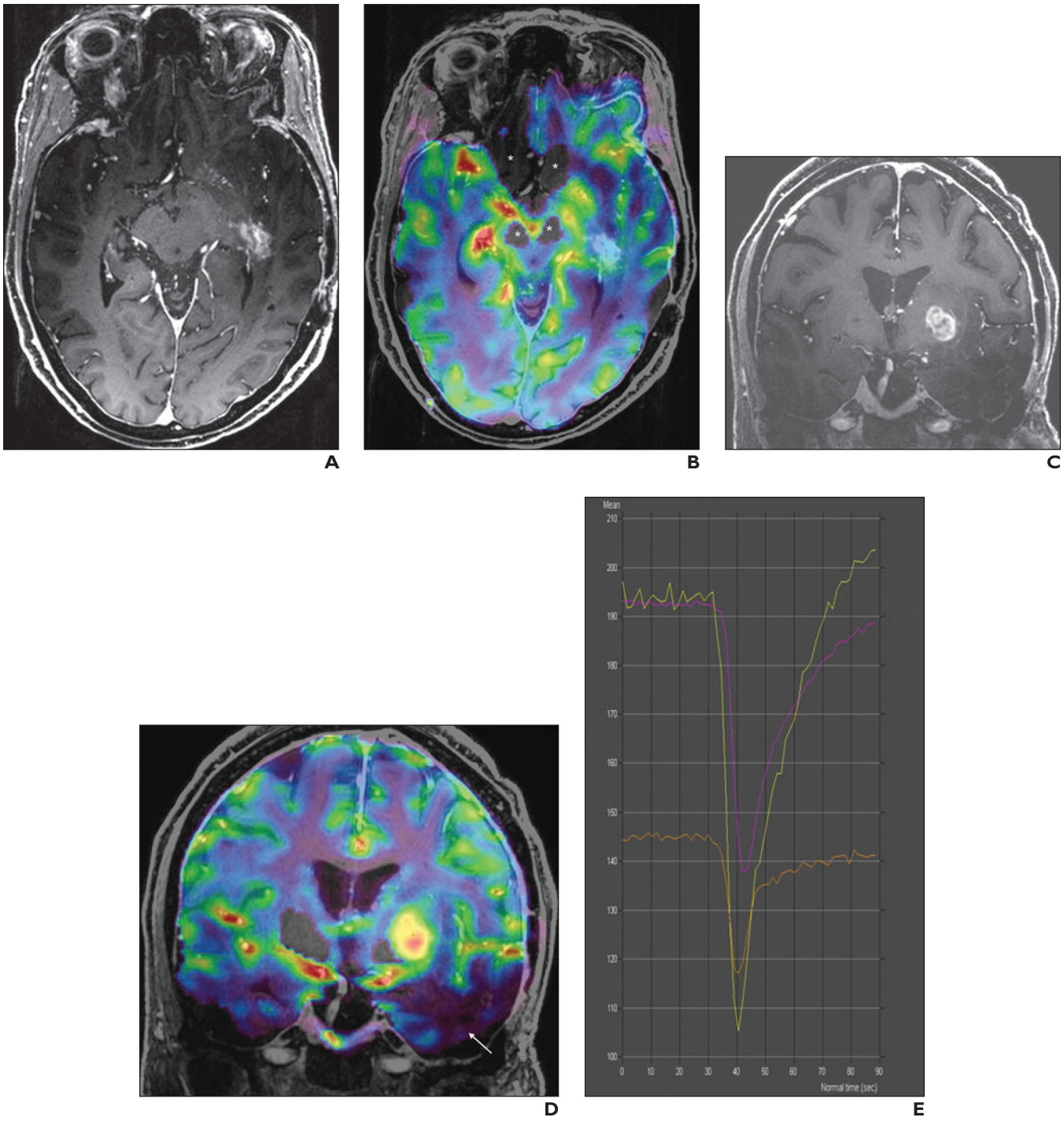

Fig. 4—.

69-year-old woman with history of left temporal lobe low-grade oligoastrocytoma who had undergone resection and radiotherapy. Follow-up imaging was stable until new patchy enhancement was identified in left temporal lobe 16 years after surgery. This patchy enhancement remained stable on follow-up MRI examinations for 2 years. Patient then

developed new seizures and was referred for 7-T MRI with dynamic susceptibility contrast perfusion imaging.

A, Axial contrast-enhanced 3D T1-weighted MP-RAGE image shows patchy enhancing area in left temporal lobe, which was stable in comparison with prior examinations (not shown).

B, Fused axial 3D T1-weighted MP-RAGE and relative cerebral blood volume (rCBV) map shows lesion (*blue*). Perfusion signal is lacking near skull base (*asterisks*), attributable to susceptibility effects.

C, Coronal contrast-enhanced 3D T1-weighted MP-RAGE image shows new enhancing mass in left basal ganglia.

D, Coronal fused 3D T1-weighted MP-RAGE and rCBV map image shows markedly increased perfusion (*yellow, red*) corresponding to enhancing lesion in **C**. Because rCBV map is obtained with thin slices (1.6 mm), coronal reformatted images do not show significant staircase artifact. Perfusion signal is lacking near lower portions of temporal lobes (*arrow*) owing to susceptibility effects.

E, Screenshot shows perfusion graph. Yellow line indicates left basal ganglion lesion (corresponding to **D**, mean rCBV, 474); purple line indicates left temporal lobe lesion (corresponding to **B**, mean rCBV, 223); orange line indicates normal-appearing contralateral white matter (mean rCBV, 139). Ratio of mean rCBV between lesion and contralateral white matter is 3.4 for left basal ganglion lesion and 1.6 for left temporal lobe lesion. On basis of perfusion data, left basal ganglion lesion was considered to represent malignant tumor, and left temporal lobe lesion was considered to represent radiation necrosis. Patient declined biopsy of left basal ganglion lesion and was referred to hospice.

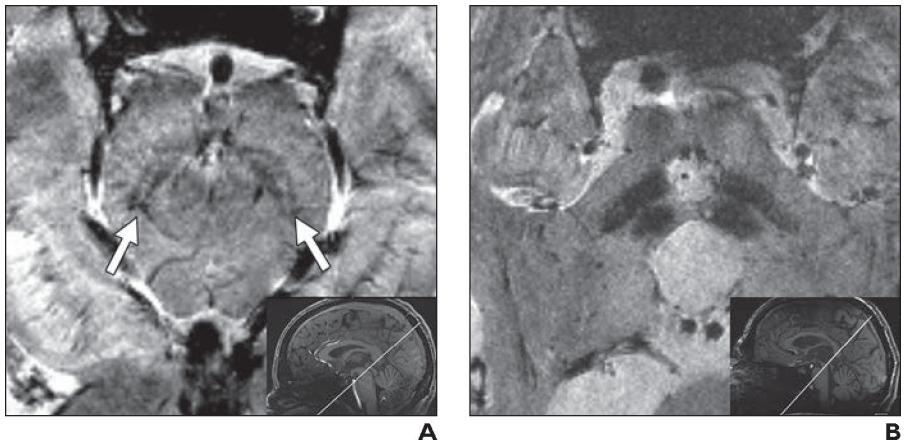

Fig. 5—.

"Loss of swallowtail" sign.

A, 32-year-old healthy man who volunteered to undergo 7-T brain MRI. Oblique axial 7-T T2*-weighted image (limited anatomic coverage; 42 slices of midbrain; slice thickness, 1 mm; matrix, 448 × 448; acquisition time, 4.34 minutes; FOV, 180 mm; voxel size, 0.4 × 0.4 × 1.0 mm; TR/TE, 1140/20; acceleration factor, GRAPPA 2; interpolation off) obtained perpendicular to axis of mesencephalon (*inset*) clearly shows bilateral swallowtail sign (normal hyperintensity within inner inferior and posterolateral part of substantial nigra) (*arrows*).

B, 61-year-old man with typical ocular findings of mild-to-moderate progressive supranuclear palsy, including frequent square wave jerks, decreased blinking rate, slowed saccades (vertical more than horizontal), and moderate vertical supranuclear palsy. Oblique axial 7-T T2*-weighted image obtained with same anatomic coverage, orientation (*inset*), and parameters as in **A** shows bilateral loss of swallowtail sign, consistent with diagnosis of progressive supranuclear palsy. Examination additionally revealed "hummingbird" sign (< 0.52 ratio of anterior-posterior diameter on midsagittal T1-weighted image of midbrain to pons [not shown]), also consistent with progressive supranuclear palsy. Dopamine transporter scan was also suggestive of progressive supranuclear palsy (not shown).

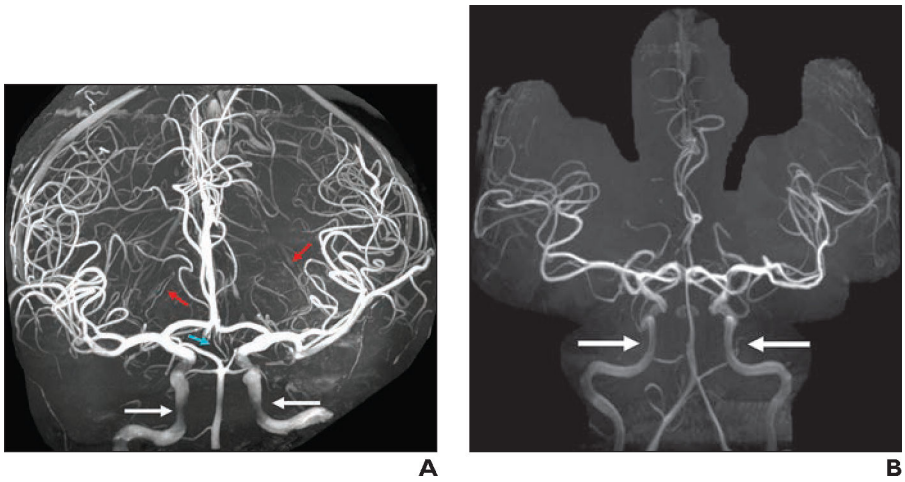

Fig. 6—.

Imaging of intracranial arteries.

A, 38-year-old healthy individual who volunteered to undergo 7-T MRI of brain. Three-dimensional maximum-intensity projection (MIP) image from 3D TOF MRA (slice thickness, 0.25 mm; matrix, 640 × 500; FOV, 180 mm; interslice distance, 18.75%; voxel size, 0.1 × 0.1 × 0.3 mm; acquisition time, 19 minutes; TR/TE, 26/7; acceleration factor, GRAPPA 2; interpolation on) shows excellent detail of intracranial arteries. Incidentally detected artery of Percheron (*turquoise arrow*) arises from right posterior cerebral artery P1 segment and exhibits early bifurcation to right and left thalamic perforators. Medial and lateral lenticulostriate arteries (*red arrows*) can be followed to thinner distal branches in basal ganglia. Cavernous internal carotid arteries (*white arrows*) are not clearly visible owing to artifact near skull base.

B, 38-year-old woman referred for brain tumor follow-up. Three-dimensional MIP image reconstructed from precontrast MP-RAGE MRA shows normal delineation of cavernous internal carotid arteries (*arrows*). This method can be used in conjunction with 3D TOF MRA for complete visualization of intracranial arterial vasculature.

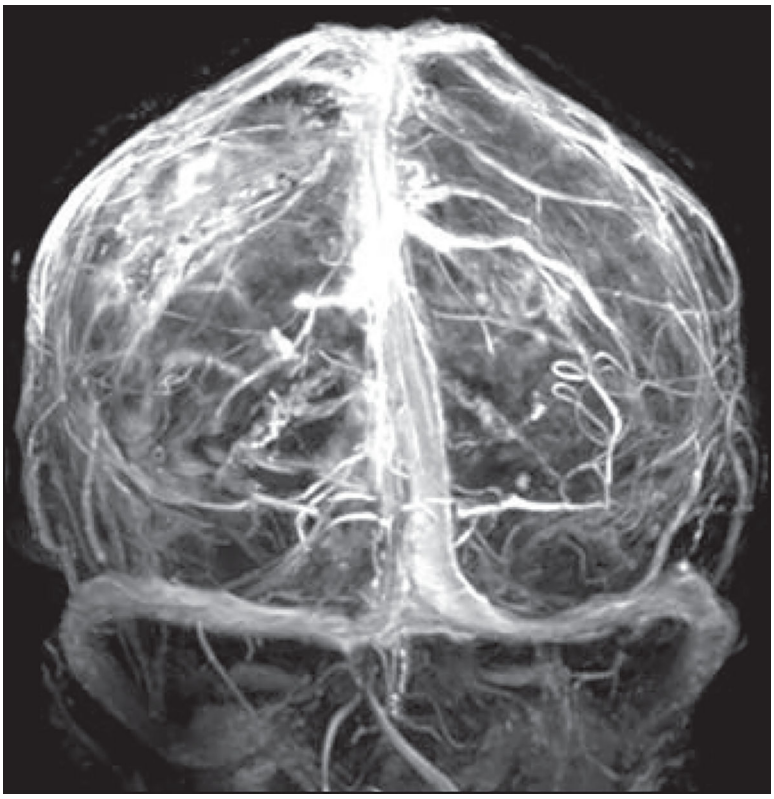

Fig. 7—.

38-year-old woman referred for brain tumor follow-up (same patient as in Fig. 6B). Three-dimensional MIP image was reconstructed from subtraction of precontrast 3D T1-weighted MP-RAGE acquisition from contrast-enhanced 3D T1-weighted MP-RAGE acquisition. Because routine sequences allow sufficient venographic evaluation, additional dedicated MR venography sequence may not be needed.

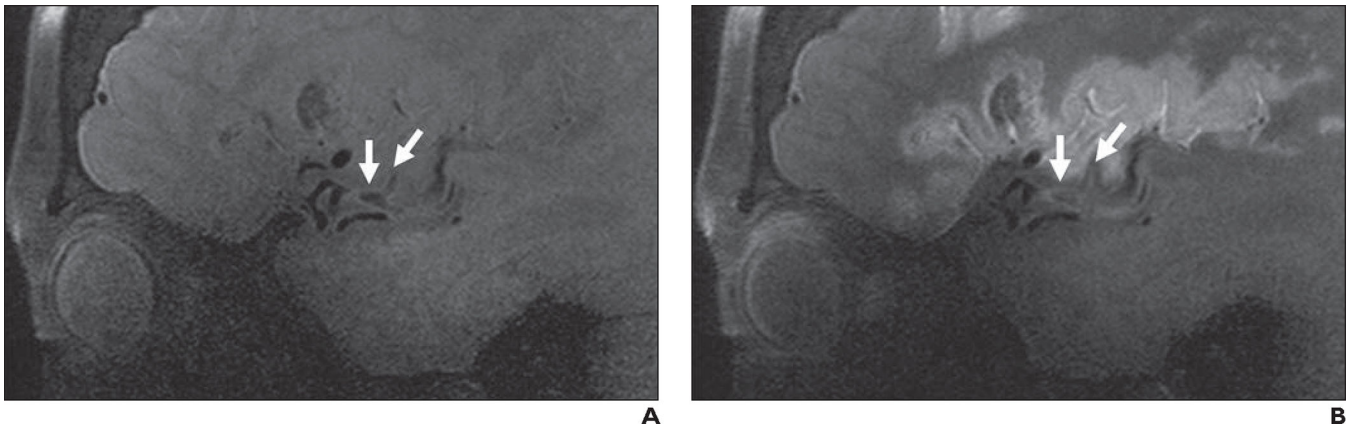

Fig. 8—.

62-year-old woman with left middle cerebral artery infarct (same patient as in Fig. 1). MRI at 7 T with vessel wall imaging was performed to exclude intracranial atherosclerosis and vasculitis. Evaluation was performed with sagittal 3D fat-saturated T1-weighted black-blood SPACE sequence (slice thickness, 0.5 mm; matrix, 272 × 272; FOV, 136 mm; interslice distance, 0%; voxel size, 0.3 × 0.3 × 0.5 mm; acquisition time, 5 minutes 6 seconds; TR/TE, 1100/23; acceleration factor, controlled aliasing in parallel imaging results in higher acceleration 3 [CAIPIRINHA 3]; interpolation on).

A and **B,** Precontrast image (**A**) and postcontrast image obtained with half dose of contrast medium (**B**) show no vasculitis or inflamed plaque. Presumed embolic thrombus is present at M2-M3 junction (Y-shaped structure [*arrows*]) and exhibits subtle signal, in contrast to low signal intensity in patent vasculature. Adjacent vessel wall exhibits accompanying mild thickening. Expected enhancing cortical laminar necrosis is also present in **B**.

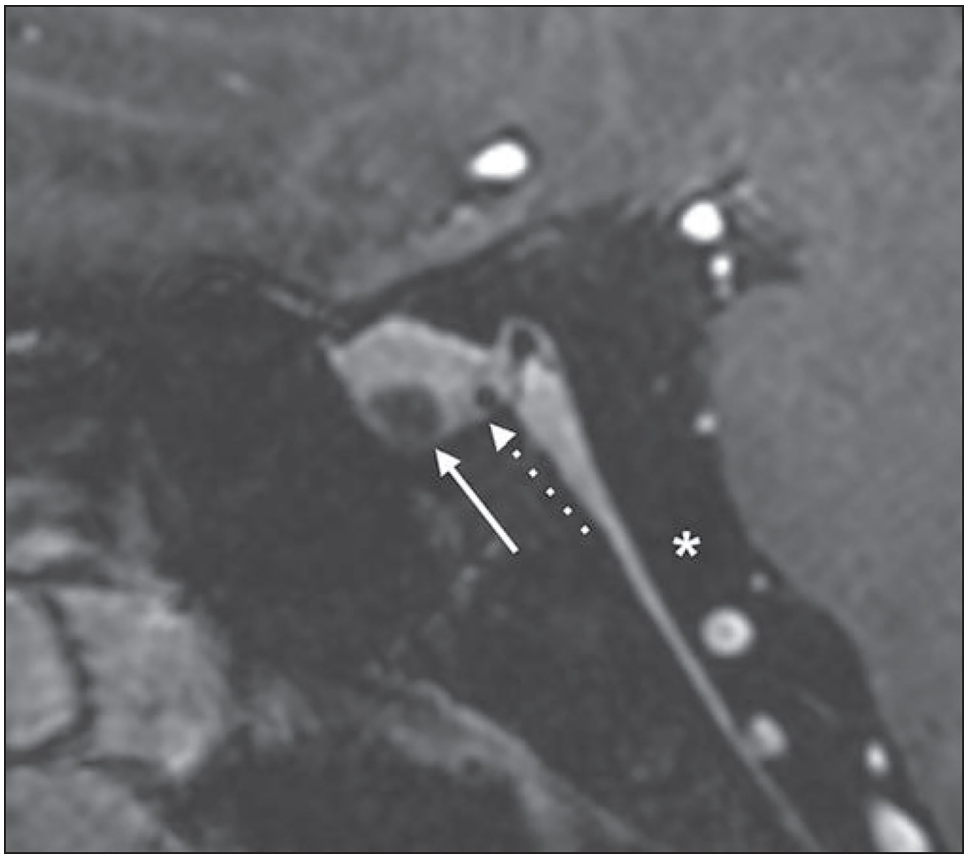

Fig. 9—.

51-year-old woman with known nonfunctioning hemorrhagic pituitary microadenoma who underwent follow-up evaluation with 7-T MRI. Sagittal postcontrast 3D T1-weighted MP-RAGE image shows known nonenhancing microadenoma (*solid arrow*) and new lesion (*dotted arrow*), which is located between adenohypophysis and neurohypophysis. New lesion has T1 hypointensity that is similar to CSF signal (*asterisk*) and was thus favored to represent incidental Rathke cleft cyst.

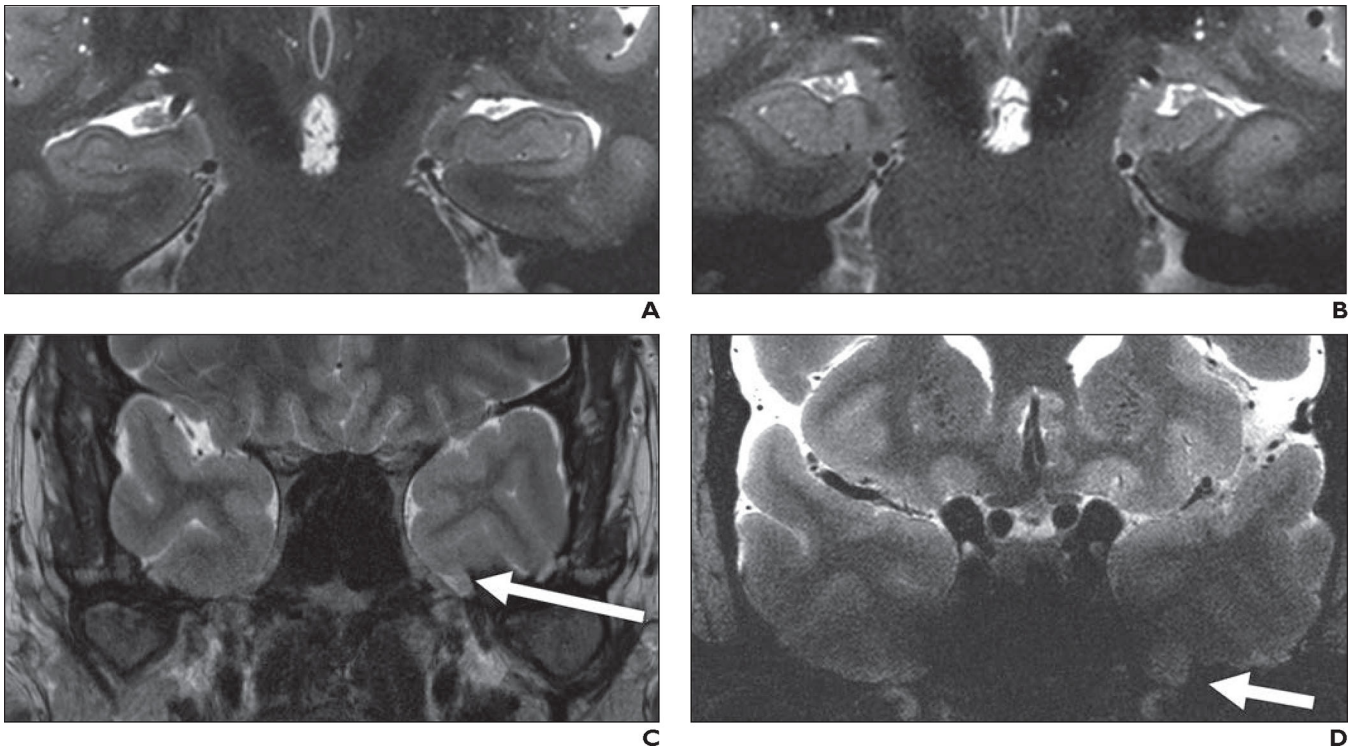

Fig. 10—.

Epilepsy and hippocampal imaging.

A, 48-year-old healthy man who volunteered to undergo 7-T brain MRI. Oblique coronal T2-weighted turbo spin-echo (TSE) image (slice thickness, 1.5 mm; FOV, 0.2 × 0.2 mm) shows excellent anatomic detail of hippocampus bilaterally.

B, 35-year-old man with complex partial seizures for 13 years and left temporal spike-wave complexes on electroencephalography (EEG). Oblique coronal 7-T T2-weighted TSE image obtained with same parameters and at comparable slice position as **A** shows small left hippocampus with loss of interdigitations in comparison with contralateral normal side, consistent with mesial temporal sclerosis.

C and **D,** 35-year-old man with complex partial seizures from left temporal lobe per EEG (different patient from **B**). Oblique coronal 3-T T2-weighted image (**C**) shows left encephalocele (*arrow*, **C**), which was suspected cause of seizures. Oblique coronal 7-T T2-weighted TSE image (**D**) was unable to clearly show left temporal encephalocele despite use of dielectric pads and neck extension; encephalocele (*arrow*, **D**) was identified only after retrospective review of prior 3-T MRI (**C**).

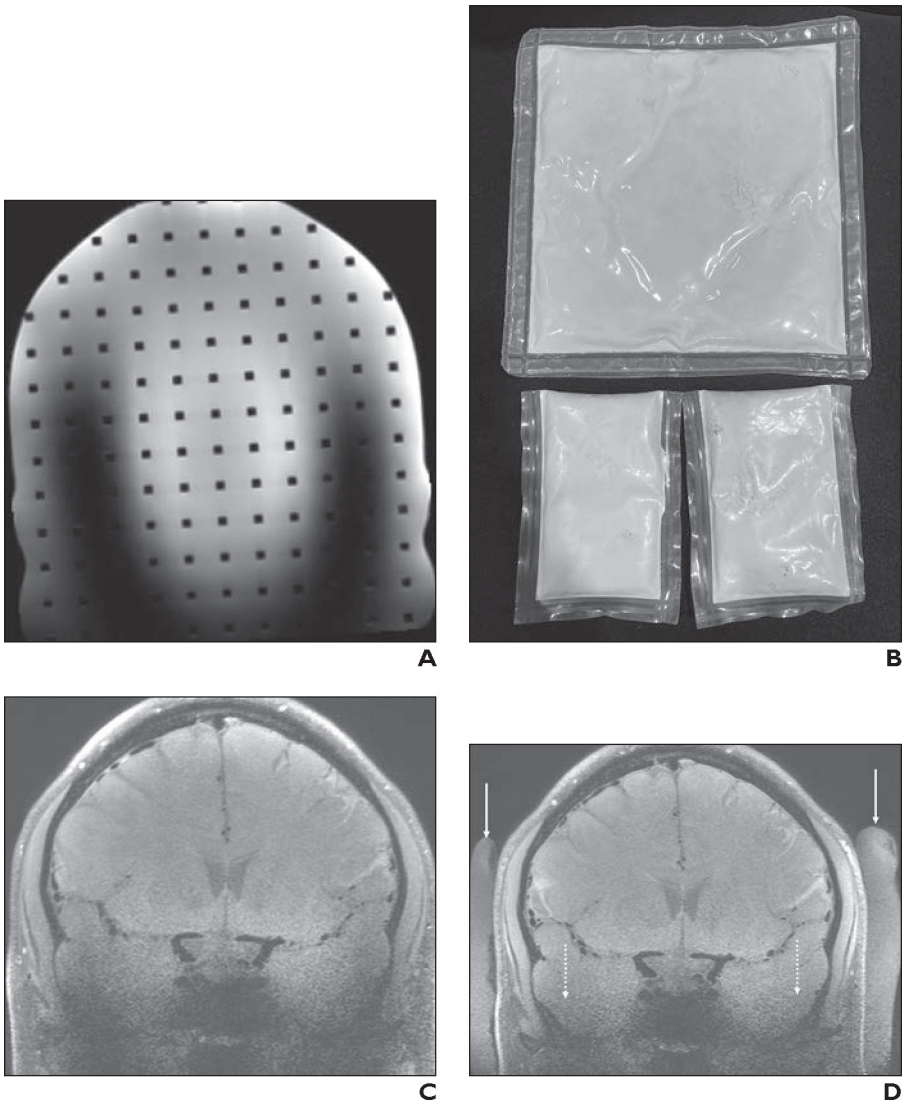

Fig. 11—.

Transmit B_1 inhomogeneity artifacts.

A, Coronal 3D 7-T T2-weighted SPACE MR image of head phantom obtained with 1-channel transmit/32-channel receive array head coil shows U-shaped region of poor signal in *z*-axis caused by B_1 inhomogeneity artifacts.

B, Photograph shows dielectric pads. Because of its large size, commercially available dielectric pad (*top*) typically can be placed only in suboccipital region. Smaller dielectric pads made in house (*bottom*) are easier to place in certain areas, such as temporal region.

C and **D,** 40-year-old healthy man who volunteered to undergo 7-T brain MRI. Coronal 3D T1-weighted SPACE images were obtained at level of carotid terminus with black-blood vessel wall imaging sequence without (**C**) and with (**D**) dielectric pads placed along right and left lateral aspects of head. Whereas commercially available pad is not visible on MRI, in-house dielectric pads (*solid arrows*, **D**) are. Use of dielectric pads markedly improves SNR of parenchyma near lower skull base (*dotted arrows*, **D**) and improves delineation

of bony structures, secondary to decreased B_1 artifacts. However, hypointense signal near sphenoid sinuses persists after placement of dielectric pads.

TABLE 1:

Protocol for Routine 7-T Brain MRI Without IV Contrast Medium

Sequence	Plane	Slice Thickness (mm)	Matrix	FOV (mm)	Interslice Distance (%)	Voxel Size (mm)	Acq Time (min:s)	TR/TE (ms)	Accel Fac	Interpolation
3D FS T1-weighted MP-RAGE	Sagittal	0.3	224 × 224	150	50	0.3 × 0.3 × 0.3	6:32	3000/2.49	GRAPPA 3	Yes
FS FLAIR	Axial	2.0	320 × 256	220	20	0.7 × 0.7 × 2.0	3:38	9000/74	GRAPPA 3	No
FS T2-weighted TSE	Axial	3.0	704 × 704	210	30	0.1 × 0.1 × 3.0	6:08	3900/61	GRAPPA 3	Yes
T2*-weighted[a]	Axial	1.5	620 × 620	210	0	0.2 × 0.2 × 1.5	9.35	1080/20	GRAPPA 3	No
DWI RESOLVE	Axial	2.0	192 × 144	230	20	1.2 × 1.2 × 2.0	2:49	6200/46 and 72	Slice accel 3	No
SWI	Axial	1.4	640 × 640	220	20	0.2 × 0.2 × 1.4	6:28	22/15	GRAPPA 3	Yes

Note—Protocol is used to evaluate for CNS pathology in such settings as headache, trauma, dizziness, confusion, dementia, and transient ischemic attack and in situations when IV contrast media are contraindicated. Total acquisition time is approximately 25 minutes. Acq = acquisition, Accel Fac = acceleration factor, FS = fat-saturated, TSE = turbo spin-echo, RESOLVE = readout segmentation of long variable echo trains, SWI = susceptibility-weighted imaging.

[a]Optional; susceptibility effect same as for SWI; T2 signal identical to that of FS T2-weighted TSE. Sequence may thus be performed in place of separate dedicated FS T2-weighted TSE and SWI acquisitions, although the sequence may be more challenging to perform given its long acquisition time.

AJR Am J Roentgenol. Author manuscript; available in PMC 2024 January 30.

TABLE 2:

Brain Tumor and Radiotherapy Planning Protocols for 7-T Brain MRI With and Without IV Contrast Medium

Sequence	Plane	Slice Thickness (mm)	Matrix	FOV (mm)	Interslice Distance (%)	Voxel Size (mm)	Acq Time (min:s)	TR/TE (ms)	Accel Fac	Interpolation
3D FS T1-weighted MP-RAGE	Sagittal	0.3	224 × 224	150	50	0.3 × 0.3 × 0.3	6:32	3000/2.49	GRAPPA 3	Yes
FS FLAIR	Axial	2.0	320 × 256	220	20	0.7 × 0.7 × 2.0	3:38	9000/74	GRAPPA 3	No
3D FLAIR SPACE[a]	Sagittal	0.6	272 × 272	160	NA	0.6 × 0.6 × 0.6	13:14	9000/248	GRAPPA 3	No
FS T2-weighted TSE	Axial	3.0	704 × 704	210	30	0.1 × 0.1 × 3.0	6:08	3900/61	GRAPPA 3	Yes
SWI	Axial	1.4	640 × 640	220	20	0.2 × 0.2 × 1.4	6:28	22/15	GRAPPA 3	Yes
3D T2-weighted SPACE[b]	Sagittal	0.8	224 × 224	180	NA	0.8 × 0.8 × 0.8	7:50	5420/118	CAIPIRINHA 3	No
After IV injection of contrast medium (0.05 mL/kg) followed by normal saline flush (10 mL) IV, both at 2 mL/s										
DSC perfusion[a,c]	Axial	1.6	146 × 146	225	0	1.5 × 1.5 × 1.6	3:24	1500/24	Slice accel 3	No
DWI RESOLVE	Axial	2.0	192 × 144	230	20	1.2 × 1.2 × 2.0	2:49	6200/46 and 72	Slice accel 3	No
3D FS T1-weighted MP-RAGE	Sagittal	0.3	224 × 224	150	50	0.3 × 0.3 × 0.3	6:32	3000/2.49	GRAPPA 3	Yes
3D FS T1-weighted MP-RAGE[b,d]	Sagittal	0.6	224 × 224	150	50	0.6 × 0.6 × 0.6	6:32	3000/2.49	GRAPPA 3	No

Note—Total acquisition time is approximately 48 minutes for brain tumor protocol and approximately 30 minutes for radiotherapy planning protocol. Acq = acquisition, Accel Fac = acceleration factor, FS = fat-saturated, NA = not applicable, TSE = turbo spin-echo, SWI = susceptibility-weighted imaging, CAIPIRINHA = controlled aliasing in parallel imaging results in higher acceleration, DSC = dynamic susceptibility contrast, RESOLVE = readout segmentation of long variable echo trains.

[a] Sequence included in both brain tumor protocol and radiotherapy planning protocol.

[b] Sequence included only in radiotherapy planning protocol.

[c] Optional sequence, performed at discretion of ordering clinician and neuroradiologist.

[d] Included 3D distortion correction algorithm.

TABLE 3:

Multiple Sclerosis and Other Demyelinating Diseases Protocol for 7-T Brain MRI With and Without IV Contrast Medium

Sequence	Plane	Slice Thickness (mm)	Matrix	FOV (mm)	Interslice Distance (%)	Voxel Size (mm)	Acq Time (min:s)	TR/TE (ms)	Accel Fac	Interpolation
3D FS T1-weighted MP-RAGE	Sagittal	0.3	224 × 224	150	50	0.3 × 0.3 × 0.3	6:32	3000/2.42	GRAPPA 3	Yes
FS FLAIR	Axial	2.0	320 × 256	220	20	0.7 × 0.7 × 2.0	3:38	9000/74	GRAPPA 3	No
3D FLAIR SPACE	Sagittal	0.8	192 × 173	160	NA	0.8 × 0.8 × 0.8	7:14	9000/249	GRAPPA 3	No
3D DIR SPACE	Sagittal	0.9	160 × 160	170	NA	0.5 × 0.5 × 0.9	8:26	8000/321	GRAPPA 2	Yes
FS T2-weighted TSE[a]	Axial	1.5	704 × 704	210	30	0.1 × 0.1 × 1.5	6:08 (×2)	3900/61	GRAPPA 3	Yes
SWI	Axial	1.4	640 × 640	220	20	0.2 × 0.2 × 14	6:28	22/15	GRAPPA 3	Yes
After IV injection of contrast medium (0.05 mL/kg) followed by normal saline flush (10 mL) IV, both at 2 mL/s										
DWI RESOLVE	Sagittal	2.0	192 × 144	230	20	1.2 × 1.2 × 2.0	2:49	6200/46 and 72	Slice accel 3	No
3D FS T1-weighted MP-RAGE	Sagittal	0.3	224 × 224	150	50	0.3 × 0.3 × 0.3	6:32	3000/2.42	GRAPPA 3	Yes

Note—Total acquisition time is approximately 54 minutes. Acq = acquisition, Accel Fac = acceleration factor, FS = fat-saturated, NA= not applicable, DIR = dual inversion recovery, TSE = turbo spin-echo, SWI = susceptibility-weighted imaging, RESOLVE = readout segmentation of long variable echo trains, accel = acceleration.

[a]Two separate acquisitions of the upper and lower brain.

TABLE 4:

Pituitary Protocol for 7-T Brain MRI With and Without IV Contrast Medium

Sequence	Plane	Slice Thickness (mm)	Matrix	FOV (mm)	Interslice Distance (%)	Voxel Size (mm)	Acq Time (min:s)	TR/TE (ms)	Accel Fac	Interpolation
3D FS T1-weighted MP-RAGE[a]	Sagittal	0.3	224 × 224	150	50	0.3 × 0.3 × 0.3	6:32	3000/2.49	GRAPPA 3	Yes
T1-weighted TSE[b]	Sagittal	2.0	384 × 384	160	10	0.4 × 0.4 × 2.0	5:35	500/8.5	GRAPPA 2	No
FS T2-weighted TSE[b]	Coronal[c]	1.5	704 × 704	210	20	0.2 × 0.2 × 1.5	4:41	4580/61	GRAPPA 3	Yes
T1-weighted TSE[b]	Coronal[c]	1.5	400 × 320	160	20	0.2 × 0.2 × 1.5	4:03	500/8.7	None	Yes
DWI RESOLVE[a]	Axial	2.0	192 × 144	230	20	1.2 × 1.2 × 2.0	2:49	6200/46 and 72	Slice accel 3	No
After IV injection of contrast medium (0.05 mL/kg) followed by normal saline flush (10 mL) IV, both at 2 mL/s										
Dynamic T1-weighted FLASH[b,d]	Coronal[c]	2.0	228 × 228	200	10	0.9 × 0.9 × 2.0	2:59	130/3.23	None	No
T1-weighted TSE[b]	Sagittal	2.0	368 × 368	160	10	0.4 × 0.4 × 2.0	5:35	500/8.5	GRAPPA 2	No
T1-weighted TSE[b]	Coronal[c]	1.5	400 × 320	160	20	0.2 × 0.2 × 1.5	4:03	500/8.7	None	Yes
3D FS T1-weighted MP-RAGE[a]	Sagittal	0.3	224 × 224	150	50	0.3 × 0.3 × 0.3	6:32	3000/2.49	GRAPPA 3	Yes

Note—Total acquisition time is approximately 43 minutes. Acq = acquisition, Accel Fac = acceleration factor, FS = fat-saturated, TSE = turbo spin-echo, RESOLVE = readout segmentation of long variable echo trains, accel = acceleration.

[a]Whole-brain anatomic coverage.

[b]Limited anatomic coverage, focused on the pituitary gland.

[c]Oblique plane in orientation of pituitary stalk.

[d]Optional sequence, performed at discretion of ordering clinician and neuroradiologist.

TABLE 5:

Epilepsy and Seizure Protocol for 7-T Brain MRI With and Without IV Contrast Medium

Sequence	Plane	Slice Thickness (mm)	Matrix	FOV (mm)	Interslice Distance (%)	Voxel Size (mm)	Acq Time (min:s)	TR/TE (ms)	Accel Fac	Interpolation
3D FS T1-weighted MP-RAGE	Sagittal	0.3	224 × 224	150	50	0.3 × 0.3 × 0.3	6:32	3000/2.49	GRAPPA 3	Yes
T2-weighted TSE	Coronal[a]	1.5	208 × 208	80	0	0.2 × 0.2 × 1.5	5:35	4500/90	GRAPPA 2	Yes
FLAIR	Coronal[a]	1.5	192 × 154	80	10	0.4 × 0.4 × 1.5	6:38	9000/68	GRAPPA 3	No
3D FLAIR SPACE	Sagittal	0.6	272 × 272	160	NA	0.6 × 0.6 × 0.6	13:14	9000/248	GRAPPA 3	No
3D T2-weighted SPACE	Sagittal	0.8	224 × 224	180	NA	0.8 × 0.8 × 0.8	7:26	5420/118	CAIPIRINHA 3	No
SWI	Axial	1.4	640 × 640	220	20	0.2 × 0.2 × 1.4	6:28	22/15	GRAPPA 3	Yes
After IV injection of contrast medium (0.05 mL/kg) followed by normal saline flush (10 mL) IV, both at 2 mL/s										
DSC perfusion[b]	Axial	1.6	146 × 146	225	0	1.5 × 1.5 × 1.6	3:24	1500/24	Slice accel 3	No
DWI RESOLVE	Axial	2.0	192 × 144	230	20	1.2 × 1.2 × 2.0	2:49	6200/46 and 72	Slice accel 3	No
3D FS T1-weighted MP-RAGE	Sagittal	0.3	224 × 224	150	50	0.3 × 0.3 × 0.3	6:32	3000/2.49	GRAPPA 3	Yes

Note—Total acquisition time is approximately 55 minutes. Acq = acquisition, Accel Fac = acceleration factor, FS = fat-saturated, TSE = turbo spin-echo, CAIPIRINHA = controlled aliasing in parallel imaging results in higher acceleration, SWI = susceptibility-weighted imaging, DSC = dynamic susceptibility contrast, accel = acceleration, RESOLVE = readout segmentation of long variable echo trains.

[a]Oblique plane in orientation of hippocampus.

[b]Optional sequence performed at discretion of ordering clinician and radiologist.